AFRL-AFOSR-VA-TR-2018-0404

S-Layer Directed Nanoscale Fluid Mechanics

Dietmar Pum
ZENTRUM FUER NANOBIOTECHNOLOGIE

10/16/2018
Final Report

Air Force Research Laboratory
AF Office Of Scientific Research (AFOSR)/ RTB2
Arlington, Virginia 22203
Air Force Materiel Command

REPORT DOCUMENTATION PAGE

Form Approved
OMB No. 0704-0188

1. REPORT DATE *(DD-MM-YYYY)*	**2. REPORT TYPE**	**3. DATES COVERED** *(From - To)*
12-10-2018	Final Technical	30-09-2015 - 29-09-2018

4. TITLE AND SUBTITLE
S-layer directed nanoscale fluid mechanics

5a. CONTRACT NUMBER
FA9550-15-1-0459

5b. GRANT NUMBER

5c. PROGRAM ELEMENT NUMBER

6. AUTHOR(S)
Prof. Dr. Dietmar Pum (PI)

5d. PROJECT NUMBER

5e. TASK NUMBER

5f. WORK UNIT NUMBER

7. PERFORMING ORGANIZATION NAME(S) AND ADDRESS(ES)

Department fuer Nanobiotechnologie
Universitaet fuer Bodenkultur Wien
Muthgasse 11
A1190 Vienna, Austria

8. PERFORMING ORGANIZATION REPORT NUMBER

9. SPONSORING / MONITORING AGENCY NAME(S) AND ADDRESS(ES)

AFOSR
875 N. Randolph St.
Arlington, VA 22203

10. SPONSOR/MONITOR'S ACRONYM(S)

11. SPONSOR/MONITOR'S REPORT NUMBER(S)

12. DISTRIBUTION / AVAILABILITY STATEMENT

A (approved for public release; distribution unlimited)

13. SUPPLEMENTARY NOTES

14. ABSTRACT

Two-dimensional crystalline S(urface)-layers are the most commonly observed cell surface structures in prokaryotic organisms (Bacteria and Archaea). Although no general biological function has been found so far, many of the specific functions assigned to S-layers depend on the complete coverage of the bacterial cells. However, a striking feature of S-layers are their excellent anti-fouling properties as already successfully applied in microfluidic devices. In this context, we assumed that this effect may also be related to the hydrodynamic surface properties of S-layer coated bacterial cells in water. The investigation of both phenomena, anti-fouling and flow resistance in water, as benefits for the bacterial cell was the main objective of this research project. The work was based on the assumption that the water layers directly associated with the nanometric topography and surface charge distribution of the S-layer protein matrix play an important.

The change in the wetting behavior of the S-layer depending on the dried or wet state and, in particular, on the crystallinity of the layer were the two main results of the contact angle measurements. Furtheron, the anti-fouling properties of S-layers were further confirmed by binding experiments with serum albumin.

We continued our investigation of the non-classical pathway of S-layer crystal growth on solid supports. QCMD and real time AFM demonstrated that adsorption of S-layer monomers from solution is completed within 5 minutes, the amount of adsorbed protein was sufficient for the generation of a complete monolayer but prolonged incubation in buffer containing $CaCl_2$ mandatory for conversion into the crystalline structure. In this context, we had been able to establish micro molding in capillaries and micro contact printing as standard procedures for making patterned S-layer lattices. Moreover, studies on the role of Fe^{2+} ions for the reassembly process confirmed the paleo-geo-chemical hypothesis by which a simple protein membrane generated in the presence of Fe^{2+} would fulfill barrier and supporting functions in an early (anaerobic) stage of biological evolution.

The hydrodynamic surface properties of S-layers were investigated by classical rheological techniques, drag experiments with an optical trap, nanoparticle tracking analysis, DLS-based optical micro-rheology and real time volumetric imaging of free diffusing S-layer coated microparticles. Although the differences in the flow resistances and in the diffusion coefficients, respectively, between blank and S-layer coated surfaces were extremely small it seems that the S-layer lattice increases the flow resistance. We assume a delicate balance between the anti-fouling properties, the flow resistance, and the wetting behavior of S-layers which was optimized by nature in the course of evolution. Currently we are focusing on the simulation of flow across S-layers in silico and try to develop a theoretical model which will allow us to get complete picture of the S-layer – water interface and explain the antifouling and hydrodynamic surface properties in detail.

The results of this project are primarily relevant for basic research but the achievements might provide the basis for novel developments of biocompatible non-wetting surfaces.

15. SUBJECT TERMS

S-layers, flow resistance, antifouling properties, bacterial cells

16. SECURITY CLASSIFICATION OF:			**17. LIMITATION OF ABSTRACT**	**18. NUMBER OF PAGES**	**19a. NAME OF RESPONSIBLE PERSON**
					Prof. Dr. Dietmar Pum
a. REPORT	**b. ABSTRACT**	**c. THIS PAGE**	U	39	**19b. TELEPHONE NUMBER** *(include area code)*
U	U	U			+43-1-47654-80360

Final Report

S-layer directed nanoscale fluid mechanics

Agreement Award Nr.: FA9550-15-1-0459

Reporting period: 30 Sept 2015 – 29 Sept 2018

Principal Investigator: Dietmar Pum (PI), Uwe B. Sleytr , Jose-Luis Toca-Herrera (Co-PIs)

Institution and address: Department of Nanobiotechnology
University for Natural Resources and Life Sciences Vienna
1190 Vienna, Austria

Author: Dietmar Pum (PI)

Reporting date, 12 Oct 2018

Table of content

1. Abstract

Two-dimensional crystalline S(urface)-layers are the most commonly observed cell surface structures in prokaryotic organisms (Bacteria and Archaea). Although no general biological function has been found so far, many of the specific functions assigned to S-layers depend on the complete coverage of the bacterial cells. However, a striking feature of S-layers are their excellent anti-fouling properties as already successfully applied in microfluidic devices. In this context, we assumed that this effect may also be related to the hydrodynamic surface properties of S-layer coated bacterial cells in water. The investigation of both phenomena, anti-fouling and flow resistance in water, as benefits for the bacterial cell was the main objective of this research project. The work was based on the assumption that the water layers directly associated with the nanometric topography and surface charge distribution of the S-layer protein matrix play an important.

The change in the wetting behavior of the S-layer depending on the dried or wet state and, in particular, on the crystallinity of the layer were the two main results of the contact angle measurements. Furtheron, the anti-fouling properties of S-layers were further confirmed by binding experiments with serum albumin.

We continued our investigation of the non-classical pathway of S-layer crystal growth on solid supports. QCMD and real time AFM demonstrated that adsorption of S-layer monomers from solution is completed within 5 minutes, the amount of adsorbed protein was sufficient for the generation of a complete monolayer but prolonged incubation in buffer containing $CaCl_2$ mandatory for conversion into the crystalline structure. In this context, we had been able to establish micro molding in capillaries and micro contact printing as standard procedures for making patterned S-layer lattices. Moreover, studies on the role of Fe^{2+} ions for the reassembly process confirmed the paleo-geo-chemical hypothesis by which a simple protein membrane generated in the presence of Fe^{2+} would fulfill barrier and supporting functions in an early (anaerobic) stage of biological evolution.

The hydrodynamic surface properties of S-layers were investigated by classical rheological techniques, drag experiments with an optical trap, nanoparticle tracking analysis, DLS-based optical micro-rheology and real time volumetric imaging of free diffusing S-layer coated microparticles. Although the differences in the flow resistances and in the diffusion coefficients, respectively, between blank and S-layer coated surfaces were extremely small it seems that the S-layer lattice increases the flow resistance. We assume a delicate balance between the anti-fouling properties, the flow resistance, and the wetting behavior of S-layers which was optimized by nature in the course of evolution. Currently we are focusing on the simulation of flow across S-layers *in silico* and try to develop a theoretical model which will allow us to get complete picture of the S-layer – water interface and explain the antifouling and hydrodynamic surface properties in detail.

The results of this project are primarily relevant for basic research but the achievements might provide the basis for novel developments of biocompatible non-wetting surfaces.

2. Introduction

Crystalline bacterial cell surface layer proteins (S-layer proteins) represent the outermost cell envelope component in a broad range of prokaryotes (Bacteria and Archaea) and are one of the most abundant biopolymers on earth (Fig.1.a). [1, 2] S-layers are monomolecular arrays of a single protein or glycoprotein species (M_w 40 to 200 kDa) and cover the archaeal or bacterial cell completely. Moreoever, due to their lattice design, S-layers are isoporous protein mesh works with unit cell sizes in the range of 3 to 30 nm, thicknesses of 5 to 10 nm (up to 70 nm in archaea), and pore sizes of 2 to 8 nm (Fig.1.b and c).

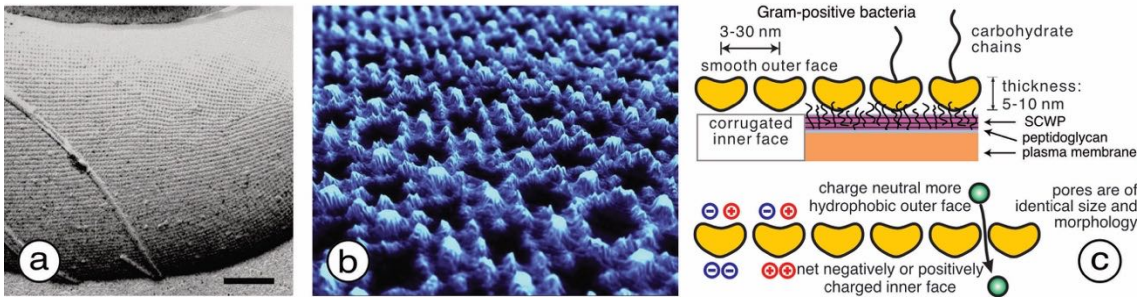

Fig.1 (a) TEM micrograph of a freeze-etched and metal shadowed preparation of a bacterial cell of the Gram-positive bacterium *Lysinibacillus sphaericus* CCM2177 with an S-layer (SbpA) as the outermost cell envelope component. The S-layer exhibits square (p4) lattice symmetry. The rope-like structures are the flagella of the bacterial cell. Bar, 200 nm. (b) AFM image of an SbpA S-layer protein monolayer on a silicon surface. Unit cell size is 13.1 x 13.1 nm. (c) Graphical summary of the cell wall and the properties of S-layers of Gram-positive bacteria.

The widespread occurrence and the high physiological expense of S-layers raise the question about the selection advantage of S-layer carrying organisms in their natural and frequently highly competitive habitats. This is because approximately 500,000 S-layer monomers are required for covering a rod-shaped bacterial cell completely necessitating the synthesis of more than 400 copies of a single polypeptide chain per second when a generation time of 20 min is assumed. [2] In this context it is interesting to remember that under optimal growth conditions for bacteria (in continuous laboratory cultures) S-layer deficient mutants, or variants possessing S-layers composed of (glyco)protein subunits with lower molecular mass, frequently outgrow wild type strains. [3-5] Since S-layers cover the surface of the whole cell as coherent layers it has been inferred that many biological functions may depend on the completeness of the covering and the structural and physicochemical repetitive uniformity down to the sub-nanometer scale. [2] For example, such a complete cell surface coverage will prevent either the attachment of specific phages or delay host immune reactions in case of pathogenic organisms.

In this context, a striking feature of many S-layers of bacteria and archaea are their excellent anti-fouling properties. This unique characteristic was first observed in electron micrographs of freeze etched preparations involving ultrafast (30,000 K/sec) vitrification of intact cells. [1, 6-9] Even when cells were harvested from complex environments or growth media containing a great variety of macromolecular components, the S-layer lattices were never masked by adsorbed molecules. It would be interesting to see whether S-layer glycosylation even amplifies this effect. [10] Moreover, detailed studies on molecular interactions and permeability using isolated S-layers or S-layer ultrafiltration membranes confirmed that the surface of the S-layer lattice in bacteria is charge neutral and thus prevents nonspecific binding of molecules and pore blocking. [11-13] Moreover, in Bacillacaea it was shown that S-layer lattices mask the net negative charge of the peptidoglycan containing layer. [3, 14, 15]

In addition, the repetitive topography of S-layers should be considered as a relevant feature affecting the hydrodynamic surface properties of bacterial cells too. It is tempting to speculate that the defined roughness of S-layer surfaces determines the flow resistance of cells in natural environments. Studies on friction flows of liquids at nanopatterned interfaces have shown that the slippage of fluids at channel boundaries is greatly increased by using surfaces that are patterned on the nanometer scale. [16] With prokaryotic organisms characterized by a large surface to volume ratio such effects should be of particular importance.

Considering the combination of the anti-fouling and hydrodynamic surface properties, the presence of S-layers may support flagella-driven cell locomotion in natural habitats (e.g. soil, mud) and thus justify the energy expense of S-layer protein synthesis. We presume that besides the more specific functions identified for S-layers of different organisms (e.g. specific interactions with molecules and cell surfaces as observed in pathogens) these features may turn out to be one of the most general ones amongst bacterial and archaeal S-layers. But, a more detailed explanation of these key properties of S-layers - taking their repetitive topography and physicochemical properties (e.g. charge distribution) on the nanometer scale into account - is still open.

The investigation of both phenomena, anti-fouling and hydrodynamic surface properties, as benefits for the bacterial cell was the main objective of this research proposal. We expected that the mutual interplay between the S-layer and the directly associated water layers might play a major role in these effects.

Biomimetic approaches copying these unique S-layer surface properties could be of great technological relevance as already shown in making use of the anti-fouling properties of S-layers in the development and fabrication of micro fluidic devices. [17-19]

3. Statement of objectives

The main goal of this research proposal was the detailed investigation of the anti-fouling and the hydrodynamic surface properties of S-layers. We assume that the S-layer modifies the structure of the first "locked-in" water layer(s) and, in this way, makes it to the liquid-repellent and slippery surface.

The following objectives and tasks were defined in the proposal:

1. Anti-fouling properties

1.1. Tilted plane experiments

Exploring different combinations of lubricants, droplets, and S-layers species.

1.2. Spinning disc

Exploring the effect of shear forces on the S-layer anti-fouling properties.

2. Nanoscale fluid mechanics

2.1 Rheological measurements

Application of rheological measurements to investigate the flow resistance of S-layer coated test objects.

2.2 *In situ* hydrodynamic lateral atomic force microscopy

Lateral force microscopy is used to investigate the hydrodynamic resistance of S-layers. As key feature, an S-layer coated micron sized colloidal tip will mimic the body of a bacterial cell.

3. Exploitation and dissemination of the results

Dissemination of results to the scientific community (publications, presentations), preparation of a comprehensive technology exploitation plan, and implementation of developed technology concepts via patent applications will be done.

Please, note: In the following *Achievements* section the individual objectives and tasks are divided into a more detailed list of items (with descriptive (sub)headings).

4. Achievements

All experiments were carried out with the S-layer protein SbpA from *Lysinibacillus sphaericus* CCM2177 (square (p4) lattice symmetry, a=13.1nm, d=9nm) in its recombinant (rSbpA) form and where specifically noted in its wild type form (wtSbpA). [20-22] In addition, for the sake of comparison, the S-layer protein SbsB from *Geobacillus stearothermophilus* PV72/p2 (oblique (p1) lattice symmetry, a=10.4nm, b=7.9nm, γ=81°, d=4.5nm; wild type) [4, 23], and SatA from *Aneurinibacillus Thermoaerophilus L420-91 (DSM 10154)* GS4 -97 (square (p4) lattice symmetry, a=10nm, d=n.d.; wild type) [24] were used as well. SatA-GS4 was chosen because it is glycosylated!

Protocols for the reassembly of the three S-layer proteins at various surfaces and interfaces in meso- and macroscopic scale are well established in our group and described elsewhere. [20, 21, 25-28]

All surfaces (silicon wafers cut into 12 x 12 mm pieces and glass cover slips) were cleaned according to standard protocols. [29]

4.1. Anti-fouling properties

4.1.1. Contact angle and tilted plane experiments

4.1.1.1. Contact angle of a sessile drop on a horizontal plane

SbpA, SbsB and SatA-GS4 S-layer proteins were recrystallized on silicon wafers overnight using standard protocols. [20, 21, 25-27] Prior to the contact angle measurements S-layer monolayers were carefully dried in a stream of dry nitrogen gas. [28, 29] Contact angles were determined with a Kruess EasyDrop instrument (Kruess, Hamburg, Germany) using 8µl MilliQ water droplets. The results are shown in Fig.2.

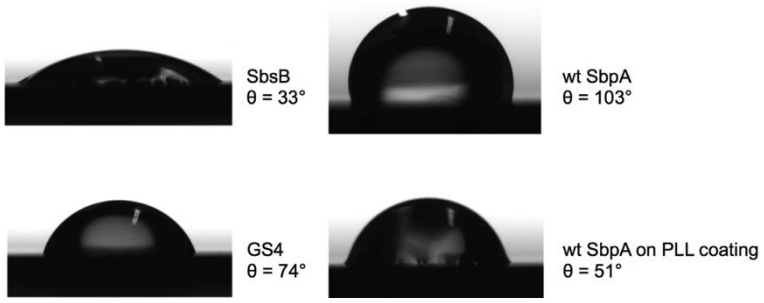

Fig.2 Results from the contact angle measurements for various dried S-layer protein monolayers (SbsB, wtSbpA, GS4, and wtSbpA on a PLL coated surface) on silicon substrates. The respective contact angles θ are denoted below.

With the exception of SbsB the S-layers are rather hydrophobic (in particular SbpA with a contact angle of 103°).

4.1.1.2. Contact angle of a sessile drop on a tilted plane

Subsequently, tilted plane experiments with S-layer coated silicon wafers were carried out in order to investigate the self-cleaning properties of S-layers (Fig.3).[30] Against our expectations, the S-layers kept the water droplets in place - even at tilting angles above 90° (not shown).

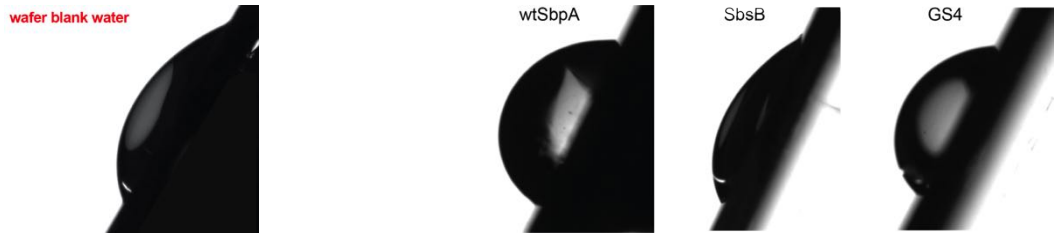

Fig.3 Water droplets on tilted (~60°) blank and S-layer coated silicon surfaces.

Surface coating	Advancing contact angle	Receding contact angle	Contact angle hysteresis
Blank	55°	37°	18°
wtSbpA	90°	63°	27°
SbsB	50°	30°	20°
GS4	80°	55°	25°

It is worth to note that contact angle hysteresis values, which indicate the adhesion of the drop towards the surface, are close together. Moreover, tilted S-layer patterned substrates (as shown here for a glass slide) were used to demonstrate the different water-retention capability of S-layer coated and blank regions (Fig.4). Water was stained with methylene blue and dropped onto the top of the tilted substrate. The water drops ran down the substrate and were held back only where the substrate was coated with wtSbpA S-layer protein.

Fig.4 Tilted S-layer patterned glass slide demonstrating the water-retention capability of the S-layer coating. For better visualization water was stained with methylene blue.

4.1.1.3. Contact angles of low and high density fluids at S-layers under water

Further experiments were carried out in a liquid cell in order to gain additional information about the anti-fouling properties of S-layers in their more natural occurring wet state. S-layer coated glass slides were submerged in water and drops of liquids with higher density (compared to water) were deposited onto and with lower density below the surface (Fig.5).

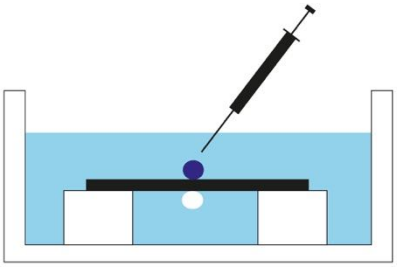

Fig.5 The S-layer coated substrate was immersed in water and a drop of either a high-density fluid was deposited from above (dark blue) or of a low-density fluid from below (white) onto the surface.

Low-density fluids (compared to water)

N pentane d =0,63 g·cm^{-3}

Hexane d = 0,66 g·cm^{-3}

Heptane d = 0,68 g·cm^{-3}

Decane d = 0,73 g·cm^{-3}

Undecan d = 0,74 g·cm^{-3}

Olive oil d = 0,91 g /cm^{-3}

High-density fluids (compared to water)

Glycerol d = 1,26 g·cm^{-3}

Ethylenglycol d = 1,11 g·cm^{-3}

Diiodomethane d = 3.325 g·cm^{-3}

Fig.6 shows the results for Diiodomethane and olive oil. The image of the olive oil droplet demonstrates the oleophobicity of S-layers.

(a) (b)

Fig.6 Contact angles of a high- and a low-density fluid on/under a wtSbpA S-layer coated glass slide in water. (a) Diiodomethane (contact angle = 140°) and (b) Olive oil (contact angle = 155°).

Unfortunately, the contact angles of alkanes on S-layers could not be measured since the surfaces were so slippery that the alkane droplets rolled off immediately.

However, no significant differences in the contact angles could be observed in comparison to uncoated, or BSA coated substrates.

4.1.1.4. Wetting behavior of dry and wet S-layers (Wilhelmy-plate method)

Glass slides

In the course of the contact angle measurements we observed that dried S-layer coated substrates show hydrophobic and wet S-layer coated substrates hydrophilic surface characteristics! Thus, this particular behavior of S-layers was investigated in detail using the *Wilhelmy-plate method.* [31]

Glass substrates were left blank on one side and coated with an S-layer on the other side (following standard protocols). A schematic drawing is shown in Fig.7 and individual images from a video shown in Fig.8.

As long as only the blank surface on both sides of the glass slide is immersed into the subphase, both sides show hydrophilic surface characteristics (Fig.7.a and Fig.8.a). When the S-layer lattice touches the air-water interface, the contact angle changes abruptly (Fig.7.b and Fig.8.b). The still dry S-layer coated surface shows hydrophobic surface characteristic as determined from the contact angle measurements (>90°) too (Fig.7.c and Fig.8.c). Upon retraction of the substrate, the now wet S-layer surface shows hydrophilic surface characteristics (Fig.7.d and Fig.8.d).

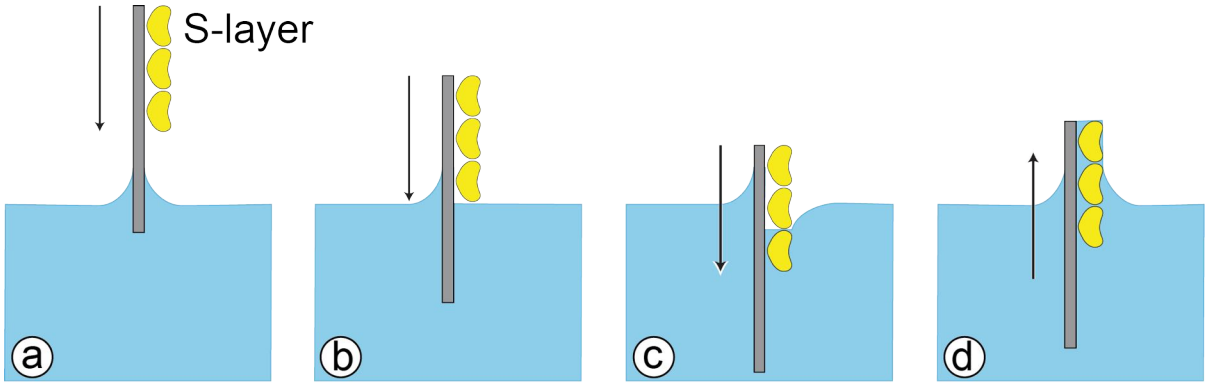

Fig.7 Schematic drawing of the Wilhelmy-plate method. The substrate (either glass or silicon) is blank on the left hand side and coated with an SbpA S-layer protein lattice on the right hand side; S-layer protein is shown in yellow. (a) Both sides of the blank substrate show hydrophilic surface characteristics. (b) When the S-layer lattice touches the air-water interface, the contact angle changes abruptly. (c) The still dry S-layer coated surface renders hydrophobic surface characteristic as determined from the contact angle (>90°). (d) Upon retraction of the substrate, the now wet S-layer shows hydrophilic surface characteristics.

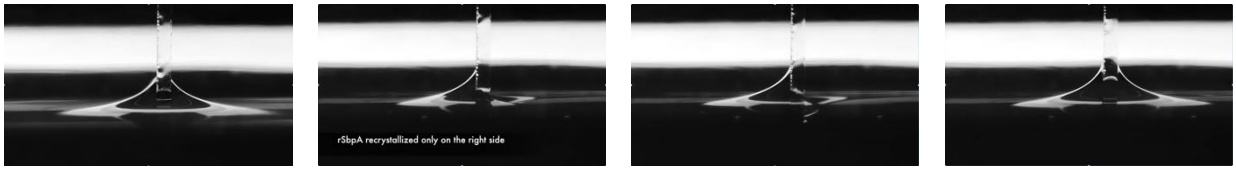

(a) (b) (c) (d)

Fig.8 Individual images taken from a video showing the wetting behavior of a blank (left side of the substrate) and an S-layer coated (right side of the substrate) glass slide. See Fig.7 for details.

The same experiments were repeated with glass slides coated with bovine serum albumin (BSA) instead of an S-layer (Fig.9). BSA was chosen since it resembles a comparable layer thickness (unit cell: 14 x 4 x 4 nm) to SbpA (unit cell: 13.1 x 13.1 x 8 nm) but does not reassemble into 2D-crystalline lattices! Upon immersion in water, contrary to the S-layer, the BSA coating shows hydrophilic surface characteristics. Nevertheless, the hydrophilicity is less compared to the blank surface (Fig.9.b).

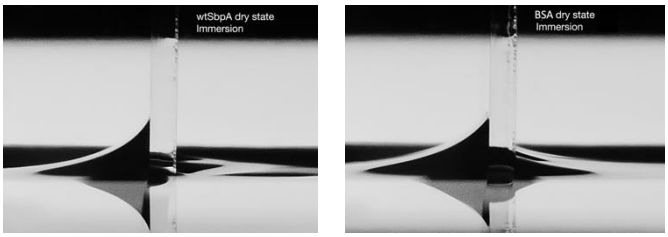

(a) (b)

Fig.9 (a) Wetting behavior of a blank (left side of the substrate) and a dried S-layer coated (right side of the substrate) glass slide upon immersion in water. The S-layer shows hydrophobic surface characteristics. (b) Same experiment as in (a) but here the S-layer was replaced by a bovine serum albumin (BSA) coating. The BSA coating shows hydrophilic surface characteristics also in the dry state.

Silicon wafers

Experiments were also carried out with S-layers on silicon wafer substrates. These experiments yielded the same results as for the glass slides (Fig.10).

(a) (b)

Fig.10 (a) Wetting behavior of a blank (left side of the substrate) and an S-layer coated (right side of the substrate) silicon wafer upon immersion in water. (b) The S-layer shows hydrophobic surface characteristics in the dried state but (b) hydrophilic surface characteristic in the wet state upon retraction from the subphase.

4.1.1.5. Importance of the crystalline state of the S-layer lattice

Based on the observation that a monolayer of randomly oriented BSA shows hydrophilic surface characteristics we decided to determine the contact angles in the course of the S-layer lattice formation. An increase in hydrophobicity of S-layer coated silicon wafers was observed during the advancing recrystallization (Fig.11). [28] The blank silicon wafers (contact angle of 37° +/- 1.8°) were incubated with SbpA in crystallization buffer (50 µg /ml) for 5 min. After washing away unbound S-layer protein further incubation was performed in crystallization buffer (CB/CB; see *Non-classical pathway of S-layer matrix assembly* below). After 5 min of S-layer reassembly, the contact angle had changed to 66° +/- 0.7° indicating a much higher hydrophobicity. After 10 min the contact angle was in the range of 84° + / - 0.3°. Without $CaCl_2$ in the buffer, the contact angle remained at 42° + / - 0.4°, and did not change over time (Tris/Tris). When $CaCl_2$ was only present in the initial phase (for 5 min) and lacking afterwards (CB/Tris) only amorphous S-layer domains

were formed and no compact crystalline layer emerged. After 20 min the contact angle values had already reached a plateau since longer recrystallization times led only to a minor increase in hydrophobicity. Overnight incubation led to a contact angle of 98° + / - 2.7° for S-layer coated silicon wafers. These findings were in good agreement with (i) QCM-D measurements in which also after 5 min no further increase of adsorbed S-layer protein was observed but the rigidness still increased, and (ii) AFM where the lattice became visible then too. Thus, these findings may be considered as a further evidence for the change in the crystalline state (from adsorbed to crystalline) and also in the rigidity of the S-layer.

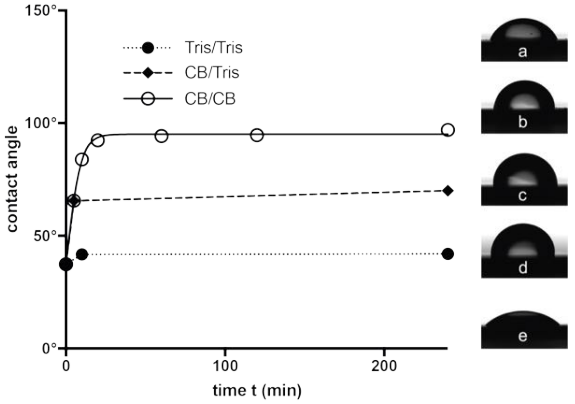

Fig.11 Contact angles of SbpA coated Si wafers over time. The contact angle of blank silicon was 37° (t=0 min). After incubation with the S-layer protein and washing away unbound protein recrystallization was allowed to take place in recrystallization buffer (CB/CB) for 5 min (a), 10 min (b), 20 min (c), 60 min, 120 min and 240 min (d), respectively. In the course of the CB/Tris path $CaCl_2$ was only present in the initial phase (for 5 min) and lacking afterwards while in the Tris/Tris path no CaCl2 was present at all. Inset (e) shows the contact angle of the S-layer coated silicon wafer without $CaCl_2$ in the buffer (after 10 min) (Tris/Tris). The contact angles were measured after air-drying the coated substrates (taken from ref. [28]).

4.1.1.6. Summary of the contact angle measurements

The change in the wetting behavior of the S-layer depending on the dried or wet state and in particular on the crystallinity of the layer are the two main results of the contact angle measurements. As summarized in the Appendix of this report, it is most likely that the *Wenzel model* or *Cassie impregnating wetting state* may best describe the wetting of the dried S-layer, in particular the *Rose petal effect* – despite the fact that the Rose petal effect was originally described for a combination of nano- and micro structures. Our conclusion is based on the observation that (i) in the course of our experiments the water drops did not roll-off from the S-layer surface when tilting up to angles > 90°, and, moreover, (ii) on the knowledge that S-layers contain high amounts of hydrophobic amino acids. [2, 21, 32]

But, this assumption may also lead to a better description of the wet S-layer surface characteristics: Upon withdrawing from the subphase the S-layer drags the water surface up. As a consequence the contact angle of the generated meniscus pretends a hydrophilic surface characteristic! In other words, it is not the S-layer protein lattice that is getting hydrophilic, it is the combined layered architecture of the nanometric S-layer (topography and surface functional groups) and the associated (locked-in) water layer which is hydrophilic!

Hydrophobic interactions are the unusually strong forces between nonpolar species interacting in aqueous medium. This phenomenon is entropically driven as structured water is released from the interfacial region. For example, the presence of single hydroxyl groups (such as the carboxylic acid group, -COOH) prevents the formation of dynamic three-dimensional hydrogen-bonded networks with water while functional groups that possess two hydroxyl groups can form such co-operative structures. [33] In this way, the hydrophobic S-layer lattice modifies the structure of the first water layers - probably repels them, but at the same time "locks them in"! This model closely resembles the concept of Slippery Liquid-Infused Porous Surfaces (termed SLIPS) as introduced by Aizenberg recently [30, 34] - but at the nanometric length scale.

4.2. Unspecific binding of serum components

The anti-fouling properties of S-layers have already been observed at S-layer coated channels in microfluidic devices. [17] This phenomenon was checked again by binding undiluted FCS (calf serum) for 30 min onto an S-layer monolayer (on a silicon surface) and visualizing the S-layer lattice by AFM. After rinsing in water, the S-layer was clearly visible again. Thus it was concluded that no FCS had been bound and the anti-fouling properties for this approach proven (Fig.12).

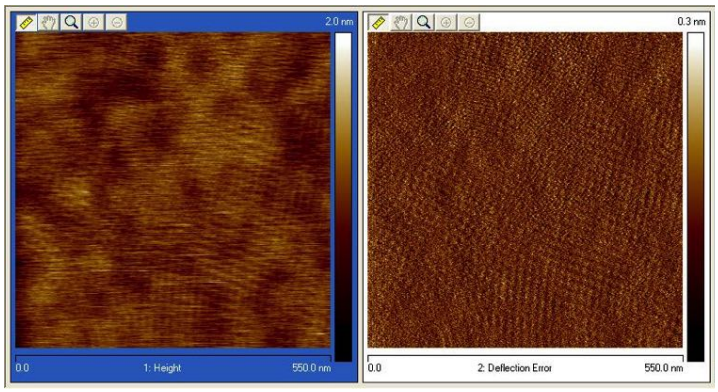

Fig.12 AFM image of an SbpA S-layer monolayer after incubation with FCS and washing. The square lattice structure of SbpA is clearly visible. No unspecific binding of serum components that interfere with the visualization of the lattice structure was found.

4.3. S-layer-hydrophobin fusion proteins

4.3.1. Hydrophobins

Hydrophobins are a group of small cysteine-rich proteins that are secreted as surface active proteins by filamentous fungi. [35] They are unique to the fungal kingdom and are essential for fungi to complete their biological cycle (coating of spores, aerial hyphae, and fruit bodies). Hydrophobins are known for their ability to self-assembly spontaneously into a hydrophobic (water-repellent) coating on surfaces including the air-water interface. The hydrophobin layer reduces the surface tension of the medium or the substrate in or on which fungi grow, allowing them to breach the air–water interface or preventing water-logging while maintaining permeability to gaseous exchange.

Hydrophobins consist of typically ~100 amino acids, show a molecular mass of 7 to 20 kDa, and are characterized by the presence of eight conserved cysteine (Cys) residues forming four disulfide bonds.

Hydrophobins are subdivided into two classes based on differences in their monomeric structure: Class I hydrophobins form a mosaic of rod-like fibrillar structures, called rodlets which are 5-10 nm in width and several hundred nanometers in length. Class II hydrophobins form films (and no rodlets) with a self-assembled hexagonally ordered structure which can be solubilized with organic solvents and detergents.

4.3.2. Bacterial hydrophobins

Bacillus subtilis is a Gram-positive soil bacterium forming biofilm colonies and pellicles that are extremely non-wetting. The biofilm matrix is composed of an exopolysaccharide and an amyloid fiber-forming protein (TasA) which assembles with the aid of a small secreted protein, termed biofilm surface layer protein (BslA). [36]

BslA is an amphiphilic protein that forms a highly hydrophobic coat around *Bacillus subtilis* biofilms, shielding the bacterial community from external aqueous solution and therefore probably from anti-microbial agents.

The biofilm formed by *Bacillus subtilis* bacterial communities features an extremely non-wetting surface, which exceeds the water repellency of Teflon! The contact angle remains nearly constant at ~135–145° in the concentration range from pure deionized water to about 80% ethanol. Findings

demonstrated that BslA is capable of self-assembly into a stable, complex higher-order film without the aid of a protein or carbohydrate partner.

Last but not least, BslA is one of the first examples of a Janus bio-nano colloid with switchable surface properties. [37]

4.3.3. Genetic engineering of an SbpA-BslA fusion protein

In this part of the project we addressed the question whether it is possible to make use of the excellent hydrophobicity of BslA for enhancing the hydrophobic surface properties of reassembled SbpA S-layer monolayers. Although a chemical binding of BslA by biochemical methods, such as activation of the carboxyl groups with 1-Ethyl-3-(3-dimethylaminopropyl)carbodiimide (EDC) and subsequent covalent binding *via* the amino groups, would have been feasible, genetic engineering of an SbpA-BslA fusion protein was considered as a preferred option since only in this way it was possible to make sure that the BslA functionality will be exposed to the environment in a dense packing resembling the lattice structure of the SbpA S-layer protein. This design principle of an oriented presentation of a fusion partner was already investigated for a broad range of S-layer fusion proteins and is based on the fact that the C-terminal truncated form of the wild type SbpA to which the BslA domain is fused is still capable to form crystalline lattices. [38] Moreover, since the S-layer moiety is attached with its N-terminal end – constituting the inner S-layer face - towards the substrate surface, it displays its fusion partner on its outer face (Fig.13).

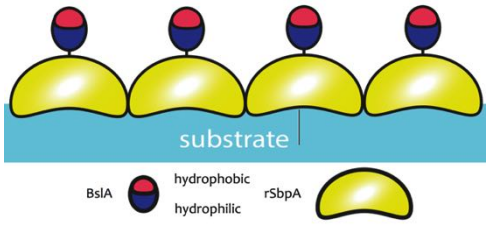

Fig.13 Schematic drawing of the SbpA-BslA layered architecture. The SbpA S-layer provides the template for the repetitive arrangement of the hydrophobin moieties and their assured orientation against the environment which leads to an increase in the hydrophobicity of the surface.

4.3.4. Cloning strategy and monolayer formation

A truncated form of $BslA_{42\text{-}181}$ with a missing signal peptide was used. This truncated form demonstrated the same surface properties as the wild type form $BslA_{1\text{-}181}$. $BslA_{42\text{-}181}$ was fused to the C-terminal truncated form $SbpA_{31\text{-}1068}$ of wtSbpA according to standard protocols [21, 39].

The final construct consisted of 1192 amino acids and had a molecular weight of 126 kDa. A schematic drawing is shown in Fig.14.

Fig.14 Schematic representation of the SbpA-BslA fusion protein

The production of a monomeric protein solution and their reassembly into ordered crystalline arrays on silicon wafers and on carbon coated TEM grids followed standard protocols. [28]

AFM and TEM were used to investigate the SbpA-BslA S-layer lattices. The crystalline lattice structure could be confirmed by Fourier domain processing. Unfortunately, more often only protein aggregates could be found but the successful visualization of SbpA-BslA monolayers may be considered as proof-of-principle for this approach (Fig.15 and 16).

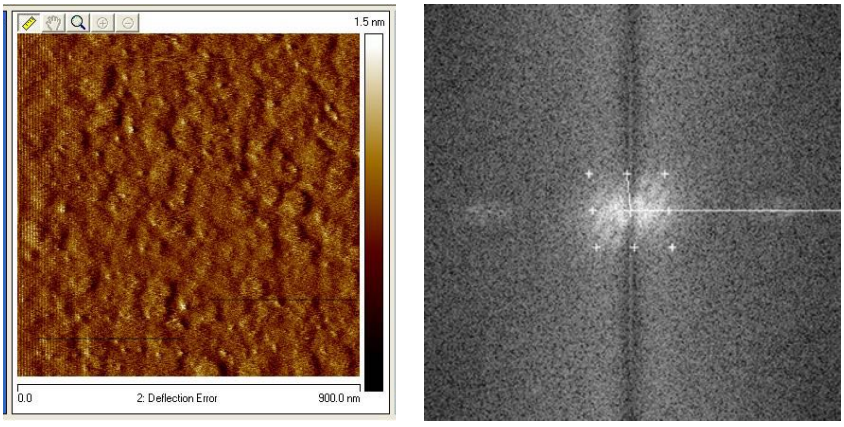

(a) (b)

Fig.15 AFM image of an SbpA-BslA monolayer on a silicon wafer (a). The lattice structure could be confirmed by Fourier domain image processing (b). The first order reflections are marked by crosses.

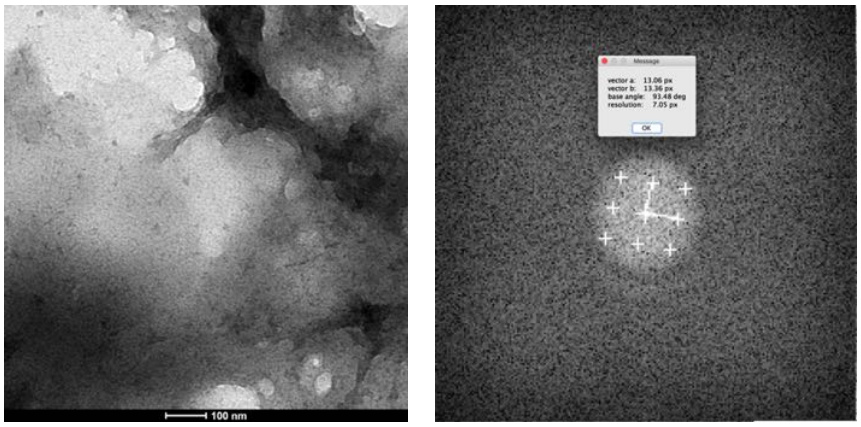

(a) (b)

Fig.16 TEM micrograph of SbpA-BslA patches and aggregates (a). The central region was used to confirm the lattice structure by Fourier domain image processing shown in (b). The inset shows the lattice parameters and resolution (1px = 1nm).

Nevertheless, an expected increase in the hydrophobic surface properties of SbpA-BslA against unmodified SbpA monolayers could not be unambiguously confirmed. In most cases contact angle measurements of dried fusion protein coated surfaces yielded values in the range of the unmodified S-layer (typically 70° - 100°) and only in a few cases contact angles of ~110° were observed.

4.3.5. Summary of the experiments with hydrophobins

The genetic work used to create an S-layer fusion protein (SbpA-BslA) with a bacterial hydrophobin moiety at the C terminus was successfully completed. The fusion protein could be successfully expressed in *E. Coli* and its reassembly properties confirmed by AFM and TEM. However, the increased hydrophobicity of the introduced bacterial hydrophobin moiety could not be unambiguously demonstrated so far which might be caused by the formation of aggregates.

4.4. Patterning of S-layer lattices

The spatial control in the formation of S-layer lattices on silicon wafers and on glass was developed for several reasons in this project but primarily for the contact angle measurements (see the *Wilhlemy-plate approach* and experiments with methylene stained water before).

4.4.1. Micro molding in capillaries (MIMIC)

SbpA S-layer protein was reassembled on hydrophobic and hydrophilic silicon wafer surfaces and patterned through the application of Polydimethylsiloxane (PDMS) molds. The molds showed

different channel widths (Fig.17.a). AFM was used to visualize MIMIC patterned SbpA S-layers on silicon wafers (Fig.17.b).

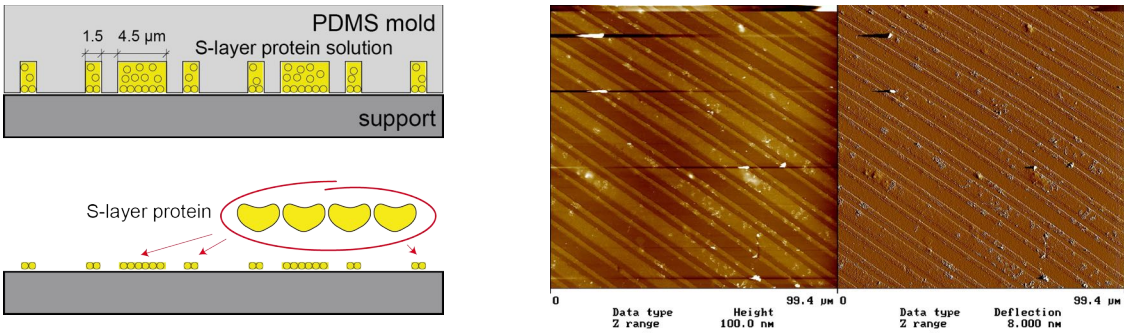

(a) (b)

Fig.17 Schematic drawing and AFM image of MIMIC patterned SbpA S-layers.

4.4.2. Micro contact printing (µCP)

Since it was not possible to successfully pattern S-layer proteins directly by µCP, it was decided to pattern blank and polyelectrolyte (PEI/PSS/PAH/PSS/PAH/PSS[1]) coated glass slides with blocking agents (StabilGuard ® or PLL-g-PEG) and subsequently incubate the entire substrate either with SbpA or with SbpA-$ZZ_{31\text{-}1068}$. SbpA-$ZZ_{31\text{-}1068}$ an S-layer fusion protein with a ZZ-domain which is the binding domain from Protein A for distinct IgG types. The patterned SbpA-$ZZ_{31\text{-}1068}$ S-layer was visualized by labeling with human IgG in the light microscope (Fig.18).

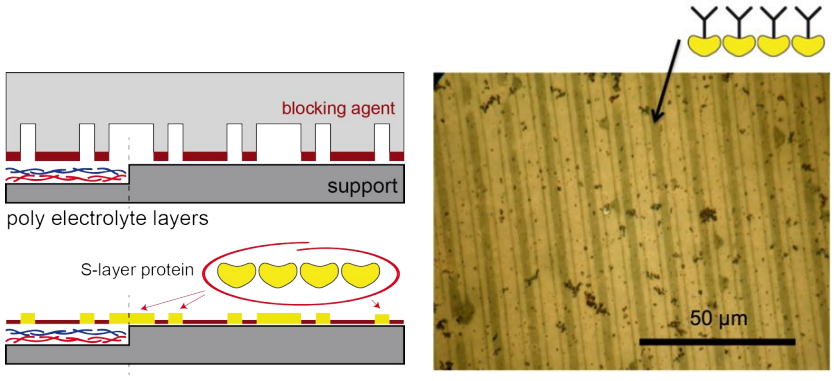

(a) (b)

Fig.18 (a) Schematic drawing of micro contact printing (uCP) of a blocking agent and subsequent S-layer protein reassembly. (b) Light microscopy image of a patterned and antibody labeled SbpA-$ZZ_{31\text{-}1068}$ protein monolayer (dark).

[1] PEI = poly(ethylene imine); PSS = poly(sodium styrene sulfonate); PAH = (poly(allylamine)) hydrochloride

The successful patterning and the formation of a crystalline lattice of SbpA was confirmed by AFM (Fig.19).

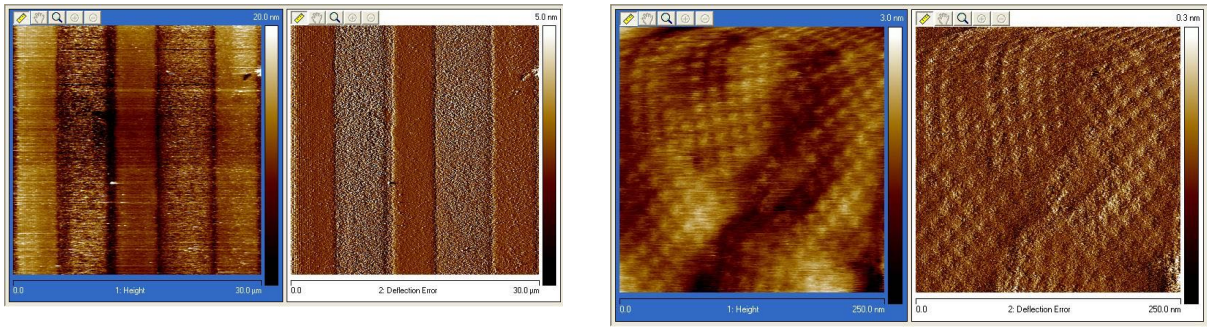

Fig.19 AFM images of a silicon wafer patterned with StabilBlot followed by incubation with SbpA and incubation in crystallization buffer overnight. The S-layer lattice structure is clearly visible in the zoomed view.

4.4.3. Summary of the patterning experiments

Micro molding in capillaries (MIMIC) is a suitable method to make S-layer patterned substrates. Micro contact printing of blocking agents is also appropriate to generate S-layer patterns on solid and – in addition – on polyelectrolyte coated substrates. Both methods were used in the course of the project.

4.5. Non-classical pathway of S-layer matrix assembly

The S-layer protein SbpA is a perfect model protein to study different crystallization pathways since the recrystallization (reassembly) process may be controlled by the presence of Ca^{2+} ions. [28, 40-42] The reassembly is entropy-driven and a fascinating example of matrix assembly following a multistage, non-classical pathway in which the process of S-layer protein folding is directly linked with assembly into extended clusters.

The recrystallization process may be separated into two distinct steps (Fig.20): (i) While adsorption of S-layer protein monomers on silicon surfaces is completed within 5 minutes and the amount of bound S-layer protein sufficient for the subsequent formation of a closed crystalline monolayer, (ii) the recrystallization process is triggered - after washing away unbound S-layer protein – by the addition of a $CaCl_2$ containing buffer solution, and completed after approximately 2 hours.

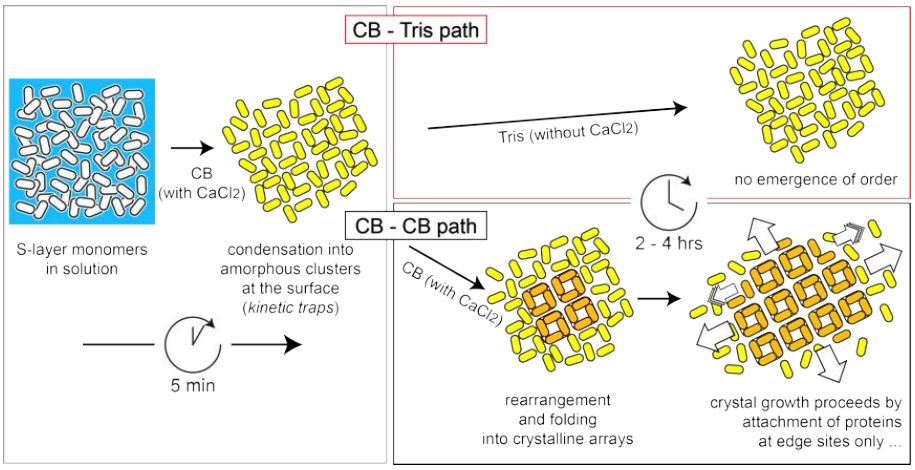

Fig.20 Schematic drawing of the two steps in the non-classical recrystallization process of the SbpA S-layer protein. Adsorption of extended S-layer protein monomers in crystallization buffer (CB; containing $CaCl_2$) from solution is completed within 5 to 10 minutes leading to an irregular but complete coverage of the surface. At the same time amorphous clusters of partially folded proteins are formed which eventually transform within 2 - 4 hours into crystalline arrays (in orange color) when crystallization buffer is added (CB – CB path). In the course of this step the S-layer proteins undergo a refolding step into a more compact tetrameric form (in orange color). Crystal growth proceeds by attachment (and refolding) of new proteins at the edge sites of the growing lattice. In contrast, no crystalline lattice is formed (even not overnight) when only Tris - and no crystallization buffer is added (CB – Tris path). (Graphics taken from ref. [28]).

The entire self-assembly process including the formation of amorphous clusters, the subsequent transformation into crystalline monomolecular arrays, and finally crystal growth into extended lattices was investigated by QCM-D and AFM. Moreover, contact angle measurements showed that the surface properties of S-layers change from hydrophilic to hydrophobic as the crystallization proceeds (see *Importance of the crystalline state of the S-layer lattice* above).

QCM-D allowed a detailed analysis and quantification of both, adsorption and subsequent recrystallization, in real time. Initial experiments with QCM-D showed that after 5 min incubation with a monomeric recombinant SbpA S-layer protein solution (50 µg/ml in crystallization buffer) no further binding of S-layer protein at the silicon wafer took place even upon excess of S-layer protein in solution. Fig.21 shows the change in frequency and dissipation for different buffer combinations (with and without Ca^{2+}-ions) for the adsorption and lattice formation of SbpA on hydrophobic silicon wafer surfaces. An unambiguous differentiation between the influence of either the addition of crystallization buffer or, alternatively, the rinsing with pure Tris buffer (identically to crystallization buffer but without Ca^{2+}; 5mM Tris; pH 9.0) was only possible by careful evaluation of variations in ΔD. For comparison, the change in Δf is not suitable for such a minute investigation. After SbpA injection, the characteristic peak in ΔD is followed by two distinctive different post-rinse behaviors characterized by either no (CB-Tris) or a gradual (CB-

CB) decay (Fig.21). The respective slopes indicate this difference within the dashed area shown in Fig.21.

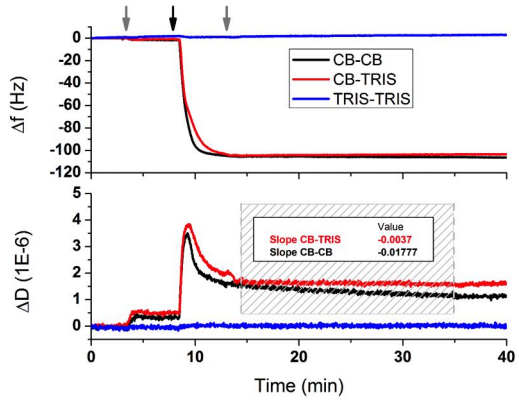

Fig.21. Real-time monitoring of SbpA protein adsorption on hydrophobic silicon QCM-D chips as recorded for frequency (top) and dissipation (bottom). Grey arrows indicate buffer injection, while the black arrow refers to injection of SbpA monomeric solution. A dashed box highlights the post-rinse region with a linear dissipation decay. Respective slopes of the fitting curves are shown in the box. (Graphics taken from ref. [28])

In this regard, the use of Tris buffer seemed to prevent the reorganization of the adsorbed protein film contrary to the presence of Ca^{2+}-ions which led towards a structure of higher rigidity within the following 20-30 minutes. A different approach to explore such a behavior is depicted in Fig.22 where in a color-coded way the SbpA-substrate interaction process may be analyzed by displaying the changes in Δf and ΔD simultaneously over time. The almost identical behavior in Δf during the first 5 minutes for both systems in the presence of Ca^{2+}, including the aforementioned transition peak at – 65 Hz, differs drastically after rinsing with different buffers. A closer look at such post-rinsing behavior (Fig.22.b) clearly indicates the continuing dense packing experienced for SbpA in crystallization buffer as compared to almost no variation recorded in Tris buffer. The slight mass uptake measured for the system under reorganization may be interpreted as a further proof of the transformation of the amorphous clusters into an array of compact tetramers, and in this way, the refolding of the monomer upon crystal formation.

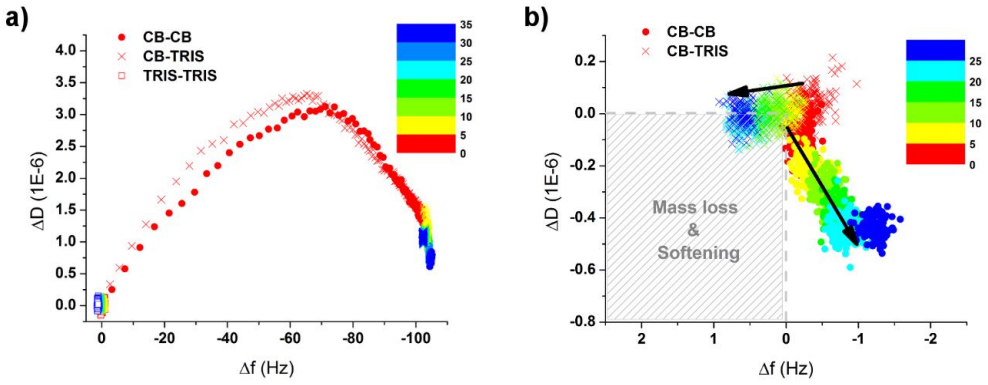

Fig.22 (a) Df plot showing the full process (adsorption + rinse) of SbpA on hydrophobic silicon wafer surfaces after short (5 min) incubation in different buffers. (b) Magnification of the post-rinse evolution of the protein films upon rinse with either Tris buffer or crystallization buffer (CB; containing Ca^{2+}-ions). The respective color scales indicate the time elapsed since the corresponding injections (in min). (Graphics taken from ref. [28]).

Based upon these findings the starting point for **AFM investigations** were hydrophobic silicon wafer surfaces incubated with SbpA (50 – 200 µg /ml crystallization buffer) for 5 or 10 min, respectively. Unbound S-layer protein was washed away and lattice formation was allowed to take place in crystallization buffer overnight. In contrast to incubation in Tris or Milli-Q water an S-layer lattice with square lattice symmetry could be clearly seen confirming the capability of the adsorbed S-layer protein to form a closed compact monolayer. Lower concentration of applied SbpA (10 and 20 µg /ml crystallization buffer; 10min) or shorter initial incubation times (1 and 2 min) did not lead to closed crystalline lattices after washing the substrates and incubation in crystallization buffer overnight. It was assumed that in this situation the incubation time was too short and the concentration of S-layer proteins too low for a sufficient amount of protein adsorbed on the silicon surface. The best experimental results were obtained with an incubation of SbpA at a concentration of 50 µg / ml crystallization buffer for 5 min. After washing away unbound S-layer protein the crystalline lattice structure could clearly be seen by AFM when the coated substrates were further incubated in crystallization buffer (average domain size 1 – 2 um). When the additional incubation was carried out in Tris buffer (without $CaCl_2$) or Milli-Q water the S-layer lattice structure could not be visualized.

Additionally, *in-situ* AFM investigations were performed in order to determine the time required to obtain the crystalline lattice after the adsorption of S-layer protein on the surface. Again, silicon wafers were incubated with SbpA (50µg / ml crystallization buffer for 5 min), washed, and subsequently inspected by AFM. Crystallization buffer was dropped onto the silicon wafer and

AFM images were taken at certain time intervals. At early incubation times (after 10, 20 and 60 min) it was challenging to visualize the crystalline lattice but after 120 and 140 min the closed crystalline monolayer exhibiting the square lattice structure could be unambiguously detected (Fig.23). It was concluded that the amount of protein adsorbed was sufficient to form a closed monolayer and although the crystalline layer emerged subsequently, the transformation of the amorphous to the crystalline state and, in this way, increase in rigidness requires a certain amount of time and the presence of Ca^{2+}-ions (e.g. $CaCl_2$). The difficulty in obtaining *in-situ* AFM images (with sufficient quality) at early stages in the assembly process is explained by the extreme softness of the protein layer at this time. This is particularly true for the very first minutes when the S-layer proteins are only loosely attached on the support and prone to movement and rotations into all possible directions by the AFM tip. Nevertheless, in the course of the subsequent reorientation against the surface and in this way stronger binding, ΔD decreases and subsequently *in-situ* AFM is able to show emerging order in the protein layer.

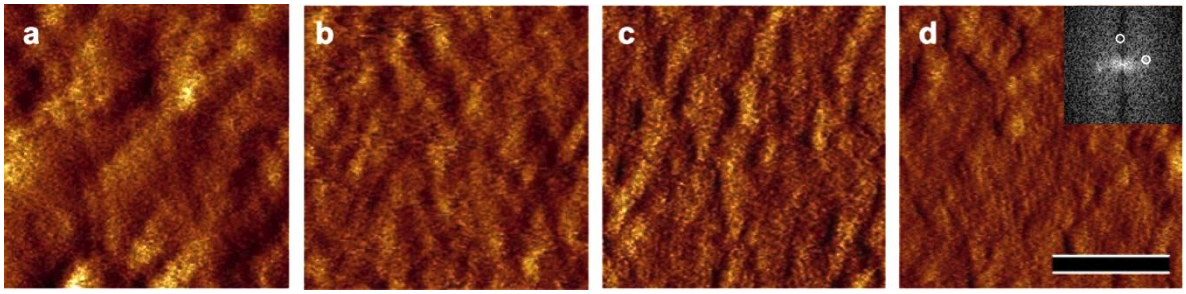

Fig.23 AFM pictures of SbpA recrystallized on a silicon wafer exploiting the two-stage process. The recombinant S-layer protein SbpA was incubated for 10 min (50 µg /ml crystallization buffer) and after a washing step incubation was prolonged. The change from the adsorbed into the crystalline state was monitored by taking images after 10 min (a), 60 min (b), 120 min (c) and 140 min (d), respectively. The square lattice structure could be visualized after 120 min incubation in crystallization buffer (bar, 200 nm). Inset shows the first order peaks of the reciprocal lattice in the Fourier spectrum corresponding to a lattice spacing of 13 nm in real space. (Graphics taken from ref. [28]).

4.5.1. Summary of the non-classical pathway of S-layer matrix assembly

Although the reassembly of S-layer proteins in solution and on solid supports is a well-established technology now for many years, the new approach in separating the reassembly process into two distinct steps (adsorption of the protein and reassembly into extended crystalline layers, respectively) is a major break-through for a broad range of bio-nanotechnological applications. Considerably smaller amounts of protein are required to completely cover a specific surface area, in particular when for example spray coating is applied. Moreover, our new approach confirms the already existing knowledge about the non-classical pathway of S-layer crystal growth. However,

it is currently under discussion how many monomeric units constitute a nucleation site with sufficient internal order to initiate lattice growth along the formed domain. [43, 44] Concentration-dependent Dynamic Light Scattering (DLS) measurements gave evidence for a "critical concentration" of association in the range of 12 to 16 monomers for the S-layer protein of *B. stearothermophilus* NRS 1536/3a (showing square (p4) lattice symmetry) [45], and accordingly *in situ* AFM yielded 8 to 60 monomers for SbpA. [40] Work will continue to address this specific question too.

4.6. Role of divalent ions for the reassembly process

Based on a stimulating discussion with Jeremiah W. Woodcock, NIST, Gaithersburg, Material Measurement Laboratory (MML) at the last AFOSR Review meeting in December 2016 we decided to check whether divalent iron cations may substitute the mandatory calcium ions in the course of the reassembly process.

4.6.1. Iron as an important micro nutrient for living organisms

Iron is an important micro nutrient for virtually all living organisms except lactic acid bacteria where manganese and cobalt are used in place of iron. Under physiological conditions iron can exist in either the **reduced ferrous** (Fe^{2+}) or the **oxidized ferric** (Fe^{3+}) form. The redox potential of Fe^{2+} /Fe^{3+} (770 mV) makes iron extremely versatile when it is incorporated into proteins as a catalytic center or as an electron carrier. Thus, iron is important for numerous biological processes which include photosynthesis, respiration, the tri-carboxylic acid cycle, oxygen transport, gene regulation, DNA biosynthesis, etc. [46]

Although iron is abundant in nature, it does not normally occur in its biologically relevant ferrous form. Under aerobic conditions the ferrous ion is unstable. Via the *Fenton reaction* ferric ion and reactive oxygen species are created. The latter can also damage biological macromolecules. Thus, the biologically available amount of iron is limited since Fe(III) is insoluble in aqueous solution (10^{-10} M soluble Fe^{3+} at physiological pH) and aggregates into insoluble ferric hydroxide.

The oxidation state of iron is interesting and important because it dramatically effects the solubility of iron in sea water. Very long ago, in the earliest days of life on earth, there was little or no oxygen (O_2). As a result, iron was most often found in the Fe(II) state. Fe(II) is quite soluble in water, so iron was probably readily available. But as atmospheric oxygen increased, iron began to prefer the Fe(III) state. Acquiring iron then became difficult and microorganisms began to develop

specialized machinery for iron acquisition. Nevertheless, it may be speculated that initially Fe^{2+} was the divalent cation which was mandatory for the reassembly of the S-layer proteins on the growing bacterial cell surface and was subsequently replaced by Ca^{2+} in the course of evolution since calcium was getting more and iron less abundant.

4.6.2. Ion specific control of the reassembly of SbpA S-layer protein

In the following experiments, we tried to replace the mandatory presence of Ca^{2+} in the reassembly process of SbpA S-layer protein by Fe^{2+} and in this way to check whether iron originally might have played the important role to trigger S-layer self-assembly. [28]

Preparation of SbpA S-layer protein and their reassembly into monolayer arrays followed standard procedures with the special feature that calcium was replaced by iron in the form of $FeCl_2 \bullet 4\ H_2O$ or $FeSO_4 \bullet 7\ H_2O$ in various buffer systems (Tris and Hepes) and concentrations (1 – 100 mM). Hepes buffer was used in a pH range between 6.0 and 8.15. Reassembly experiments were carried out according to standard protocols. [28] The oxidation state of iron may be controlled either chemically by using additives such as Dithiotreitol (DTT) or electrochemically by adjusting the electrical potential.

4.6.2.1. Chemical control

First of all, we used the chemical additive (DTT) as retardant of the naturally occurring oxidation process. The usually used $CaCl_2$ was replaced by $FeCl_2$ or $FeSO_4$ and the routinely used Tris buffer by HEPES since formation of precipitates was observed with the former (Fig.24). Furthermore, HEPES had already been reported in the literature to prevent auto-oxidation and to stabilize Fe^{2+} for a considerable length of time. [47]

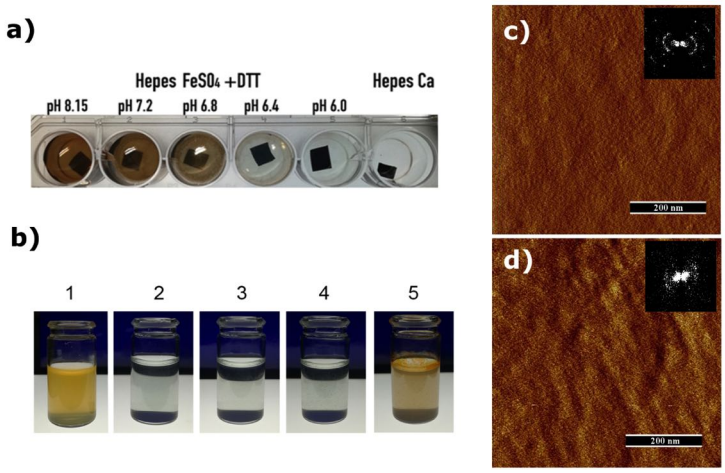

Fig.24 (a) S-layer recrystallization on hydrophobic silicon wafers in the presence of a 2 mM $FeSO_4$•7 H_2O solution in degassed 0.1M HEPES buffer (+5mM DTT) at different pH values. (b) Sample 1 acts as positive control in the absence of DTT and without previous degassing (image taken after 30 min). Time course (images 2-5) of Fe^{2+} auto-oxidation (2 mM $FeSO_4$•7 H_2O / 5 mM DTT in 0.1M HEPES at pH 6.3). Pictures were taken after 30 min (2), 180 min (3), 420 min (4) and overnight (5). (c) AFM topography micrographs of SbpA recrystallized onto silicon wafers under degassed solutions of either $FeSO_4$ (c) or $FeCl_2$ (d). The crystalline character of the S-layer patches could further be confirmed through Fourier domain analysis (insets). The multiple first order spots reflect the highly disordered paving of the small crystalline domains. Their reciprocal spacing of ca. 13 nm corresponds to the lattice constant of the SbpA S-layer lattice with its square lattice symmetry. Scale bars = 200 nm. (Graphics taken from ref. [48])

The solubility of iron strongly depends on the pH making iron less available at neutral-to-basic pH than at acidic ones. As shown in Fig.24.a HEPES solutions of both Fe(II) salts show increasing turbidity at pH values above 6.4 and the formation of large green colored aggregates which sediment at the underlying silicon surface. The appearance of such aggregates hinders the formation of a homogeneous S-layer lattice since relatively large surface areas are covered. Therefore, a final pH of 6.3 was chosen since the integrity of the SbpA protein was still maintained.

SbpA was reassembled from both $FeCl_2$ and $FeSO_4$ containing solutions over 210 min, and the resulting topographies analyzed by AFM (Fig.24.c and d). Since the S-layer lattice appears very faint and distorted (compared to its Ca^{2+} counterpart) in these images Fourier domain analysis (see insets) was used to confirm the S-layer lattice structure.

4.6.2.2. Electrical control and real time monitoring

As an alternative to the mere chemical control of the oxidation potential the electrochemical approach offered much more flexibility in terms of monitoring time series or performing classical cyclic voltammetry. Moreover, since we equipped our quartz crystal microbalance with dissipation monitoring (EQCMD) setup with an electrochemical cell (and potentiostat) we were able to

monitor the kinetics and changes in both, adsorbed mass and film viscoelasticity, as defined by variations in frequency (Δf) and dissipation (ΔD), respectively, too. [48] The resulting Δf *vs.* time and ΔD *vs.* time plots of the SbpA reassembly on hydrophobic-gold, under a controlled potential, are shown in Fig.25.

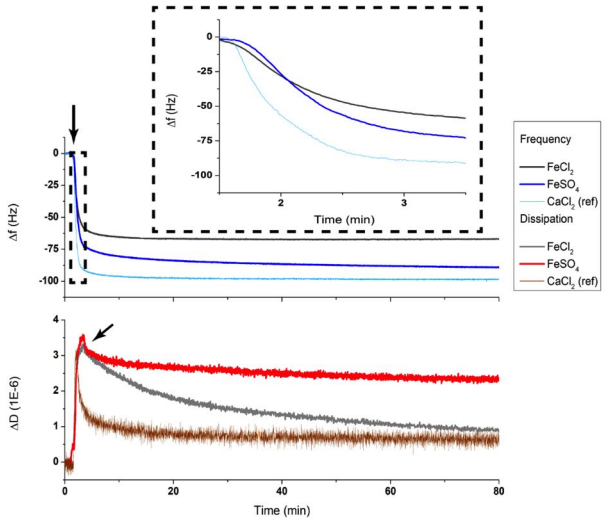

Fig.25 EQCMD measurements showing the Δf (top) and ΔD (bottom) time evolution for the recrystallization of SbpA in the presence of Fe^{2+} (chloride and sulfate) and of Ca^{2+} ions. Injection was performed on octanethiol-modified gold chips and under a controlled bulk potential (-1 V). The black arrow (above) indicates the protein injection time. The inset highlights the kinetics of the diffusion/adsorption process. The arrow below points out the appearance of the characteristic structure indicating transition peak observed in ΔD (graphics taken from ref. [48]).

The formation of the SbpA layer exhibits differences between the Ca^{2+} (acting as reference) and the Fe^{2+} triggered lattice formation - although the general trend seems to be rather similar. Overall, the most relevant outcomes may be summarized as follows: (i) the total mass adsorbed differs depending on the divalent ion (Ca^{2+} *vs.* Fe^{2+}) and also the counterion (Cl^- *vs.* SO_4^{2-}) used, (ii) in the initial state of crystal formation the structure indicating transition peak is shifted towards a more rigid layer and (iii) the kinetics of the processes are slowed down in the presence of Fe^{2+} salts. Fig.26 shows the respective AFM images taken at the end of the reassembly process (210 min).

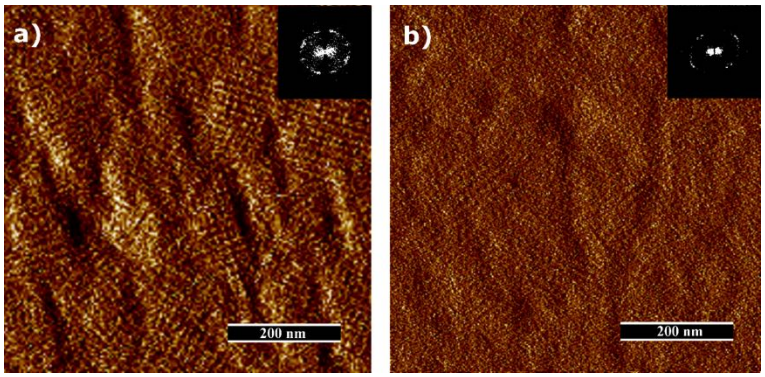

Fig.26 AFM micrograph of crystalline SbpA films onto silicon wafers under electrochemical control of the bulk potential (-1 V). The recrystallization buffer contained either $FeSO_4$ (a) or $FeCl_2$ (b). Recrystallization was checked after 210 min at RT. Insets show the resulting Fourier spectra from the respective images. Scale bars = 200 nm

4.6.2.3. Electrical stability of the Fe^{2+}-containing S-layer

Film resistances of SbpA films (in HEPES) were subsequently tested under sudden shifts in the environmental potential from -1 to +1 V (covering the Fe^{2+}/Fe^{3+} redox pair). By application of such pulses the resistance of the inner structure-trapped Fe^{2+}-ions to externally-induced oxidation could be determined. The real time response was monitored by EQCMD, as shown in Fig.27.

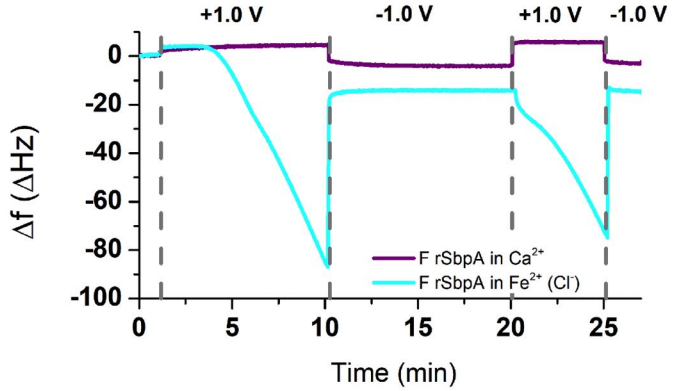

Fig.27 Fe-SbpA crystalline film electrical responsiveness. EQCMD measurements allow monitoring the real time Δf variation upon potential shifts between oxidation- (+1 V) and reduction-inducing (-1 V) conditions. A calcium-containing S-layer was used as negative control. 0.1M HEPES was used as running buffer (graphics taken from ref. [48]).

4.6.2.4. S-layer ion permeability

Cyclic Voltammetry (CV) was used to complement the observations from the previous section. Since S-layers act as protective outermost components in the cell wall (in bacteria) their ion permeability is certainly relevant (among others) too. Fig.28 shows the respective Cyclic

Voltammograms (three cycles each) recorded for Fe^{2+} induced SbpA lattice formation when sweeping the +1/-1 V range. The octanethiol-coated gold system represents the current intensity measured in the absence of a protective layer.

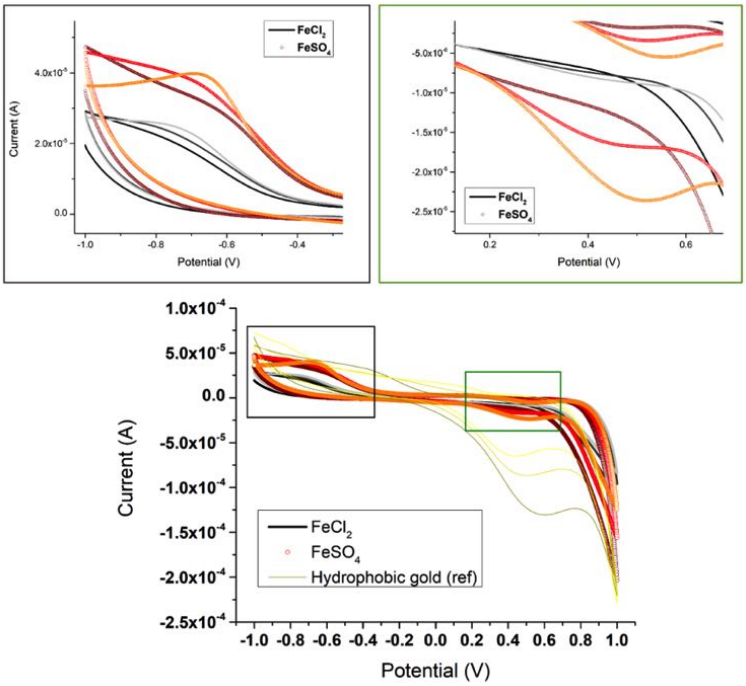

Fig.28 Cyclic Voltammetry measurements (-1 to +1 V) showing the ion permeability variation of the Fe^{2+} - containing S-layers with respect to the corresponding counterion. Experiments were performed in 0.1M HEPES and the octanethiol-gold system (yellow to green solid lines) was used as reference (graphics taken from ref. [48]).

It was shown that SbpA lattices which had been assembled in the presence of $FeCl_2$ effectively attenuate the passage of ions from the bulk phase (around a 50% lower current at the extreme potentials) compared to its sulfate-based homologous structures. Such a performance perfectly matches the QCMD/AFM results where the S-layer built in the presence of $FeSO_4$ already appeared as a more loosely packed film.

4.6.2.5. Summary of the reassembly in the presence of Fe^{2+}

This work describes for the first time the possibility of assembling fully functional S-layers from iron (II) salts ($FeCl_2$ and $FeSO_4$). Such structures could only be achieved when exerting an external control over the naturally occurring oxidation of Fe^{2+} to Fe^{3+}. In this regard, the use of a chemical (DTT, degassing) - and of an electrical (fixed bulk potential) control have demonstrated to be very efficient in acting against the oxidation of Fe^{2+} to Fe^{3+}. Formation of the respective crystalline layers was followed by QCMD offering real time monitoring over the reassembly process and

AFM demonstrating the presence of typical for SbpA lattices. $FeCl_2$ has shown to induce the formation of a very compact and smooth protein layer resembling a lattice which had been formed in the presence $CaCl_2$. For comparison, reassembly in the presence of $FeSO_4$ led to a more loose packing of the resulting lattice. Moreover, cyclic voltammetry studies have shown that the dense packing of $FeCl_2$ induced lattices led to an efficient attenuation of the ion permeability. But, most important, it has to be remembered that S-layer morphogenesis is the most simple assembly mechanism for covering the bacterial cell completely. In addition, these results confirm the paleo-geo-chemical hypothesis by which a simple protein membrane capable of dynamic growth in the presence of bivalent iron (Fe^{2+}) would fulfill barrier and supporting functions in an early (anaerobic) stage of biological evolution [2, 49].

4.7. Spinning disc

The spinning disc experiments were planned in order to study the effect of shear forces on the S-layer antifouling properties. We performed these experiments in a modified form in the course of the rheological measurements (see *Cone (disc)-type measuring device*).

4.8. Nanoscale fluid mechanics

4.8.1. Rheological measurements

The determination of the viscoelastic properties of a fluid or gel by using a rheometer is a standard technique in basic as well as applied research ranging from food and biotechnology to the development of new paintings or lubricants. Rheometry may be performed in several different ways but most commonly a stainless steel body (referred to as test object) with a polished surface is immersed in a test fluid (in a "tight-fitting" measuring cup) and rotated up to 1000 revolutions per second (Hz). The required torque is measured and eventually yields a measure of the viscoelastic properties of the fluid. The small gap between the test object and cup enhances the effect.

We made use of this technique for studying the effect of an S-layer coating (reassembled at the stainless steel body and the measuring cup) onto the flow resistance in water. For this purpose, we reversed the classical setup described before by coating the polished surface of the steel body with an S-layer and using water (or buffer) instead of a test fluid. Although the software of the instrument attributes the measured viscoelastic properties (elastic and viscous modulus) to the test fluid - which is in our case the water layer at the S-layer surface - they are actually caused by the S-layer coating!

Measurements were performed with a high-performance Rheometer (models MCR 702 and MCR 502; Paar, Graz, Austria) in the application labs of the manufacturer (Fig.29).

Fig.29 Rheometer MCR 702 (Anton Paar) shown with 2 discs and open temperature control jacket. Torque resolution is 0.1nN • m

4.8.1.1. Cylinder-type measuring device

A stainless steel cylinder and a tight-fitting measuring cup were used (Fig.30). Reassembly of SbpA S-layer protein on the stainless steel surfaces took place over night (20 ml volume; 25°C Peltier controlled). Blank experiments with deionized water were carried out before protein adsorption and after cleaning the surfaces with ethanol again. The successful monolayer formation was confirmed by AFM on steel discs (12 mm diameter) which were coated by the same SbpA S-layer protein in a parallel experiment (data not shown).

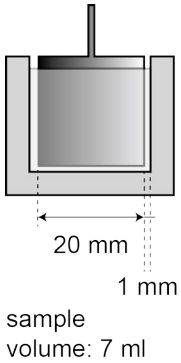

Fig.30 Schematic drawing of the cylinder setup.

The rheology measurements (Fig.31) clearly demonstrated that the S-layer coated surfaces (blue and green lines) induced a higher resistance (expressed as viscosity of surrounding medium) towards water compared to the cleaned ones (grey line). Revolutions are expressed as shear rate.

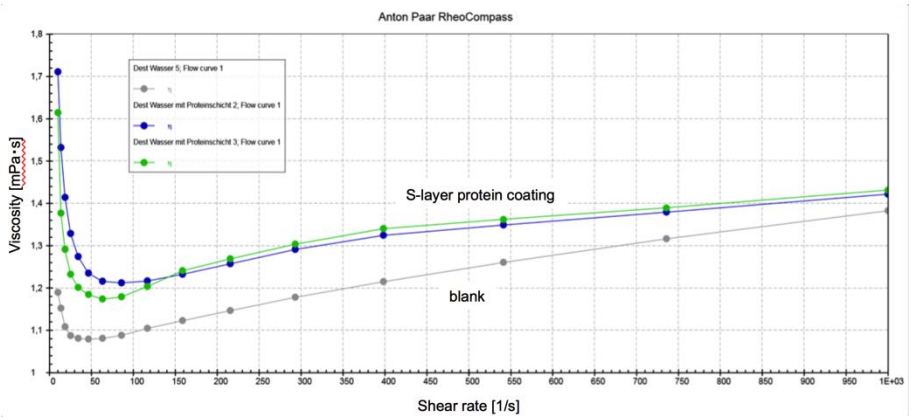

Fig.31 Viscosity versus Shear Rate (=revolutions per second): Blank (grey), and two independent measurements with SpbA (blue, green).

4.8.1.2. Cone (disc)-type measuring device

Furtheron, the effect of S-layer lattice formation on the flow resistance in water was studied in real time by injecting SbpA S-layer protein solution into a cone-type measuring device whose stainless steel surfaces were initially blank (Fig.32). Elastic and viscous moduli were recorded for 60 min with and for further 180 min without oscillating the cone (Fig.33 and Fig.34).

Blank experiments with $CaCl_2$ buffer solution were carried out before protein adsorption and after cleaning the surfaces with ethanol.

A cone-type disc was used in order to compensate the effect of the gradient in speed-of-rotation (from the center to the perimeter) onto the measurement. The angle of 0.991° is used with water as test fluid.

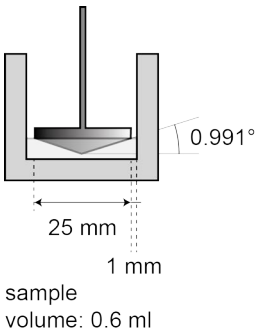

Fig.32 Schematic drawing of the cone-type setup.

The effect of the S-layer reassembly became visible ca. 6 minutes after injection of the protein solution. Both, the elastic and the viscous modulus of the water layer at the surface as induced by

the growing S-layer lattice are significantly higher compared to the blank (with Ca^{2+} only) (Fig.33). The blank values were determined within the first 5 minutes (see red double headed arrow in left panel of Fig.33). The higher viscosity of the S-layer protein solution could be neglected since no effect was seen within the first minutes after injection into the buffer.

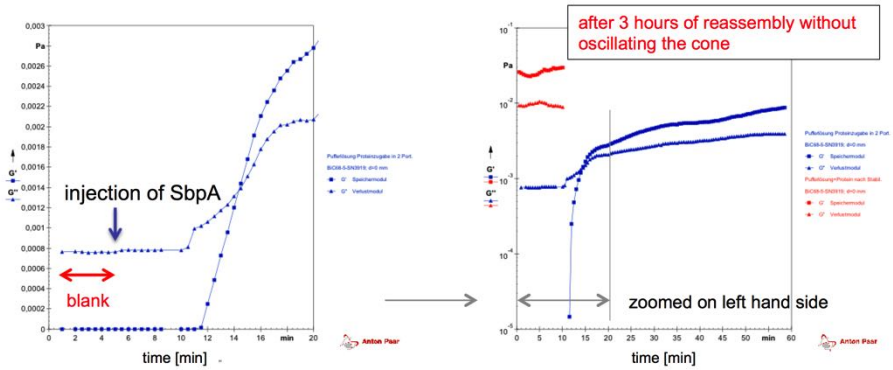

Fig.33 Time dependent change of the elastic G' (■) and viscous G" (▲) modulus of the water layer as induced during the reassembly of the S-layer protein on the surfaces of the cone and the cup. The cone was oscillated at 1 Hz. The blank values were determined within the first 5 minutes (see red double headed arrow in left panel).

Moreover, after the reassembly of the S-layer protein had been completed sc. amplitude sweep measurements were performed. In this approach the amplitude of a partial rotation of the cone is continuously increased while the angular frequency is kept constant. This approach led to a breakdown of the elastic part compared to the viscous part (Fig.34).

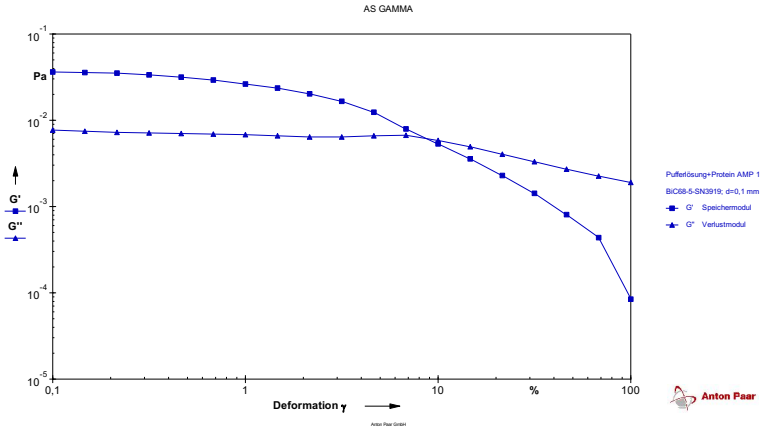

Fig.34 Elastic G' (■) and viscous G" (▲) modulus of the water layer as induced by the reassembled S-layer protein versus deformation (=amplitude of oscillation). A deformation of 100% corresponds to a full cycle.

4.8.1.3. Nanoparticle Tracking Analysis (NTA)

Dynamic light scattering allows the tracking of small particles that are in constant random thermal motion (Brownian motion). Their diffusion speed is determined by their size, as well as the temperature and viscosity of the medium. The speed or in other terms, the area which is covered within a certain time, may be determined from the speckle pattern produced by the illumination of the particles with laser light (Fig.35). Thermally driven motion of the tracer particles is intimately linked to their rheological properties.

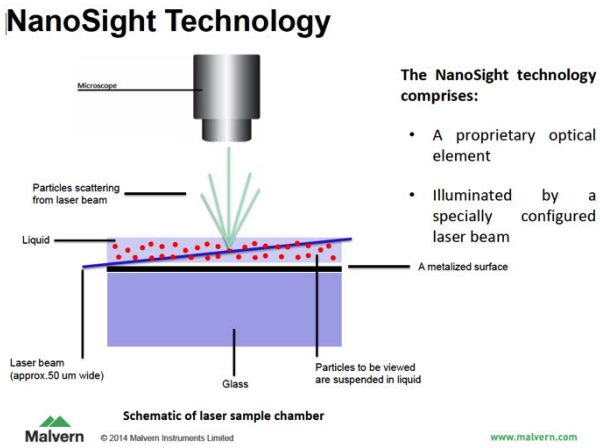

Fig.35 Schematic drawing of Nanoparticle Tracking Analysis (NTA) as implemented by the NanoSight Technology (Malvern Instruments, Malvern, UK)

In a typical workflow of NTA, the software captures a movie of the particles moving under Brownian motion, subsequently follows the movement of each particle independently and calculates its mean squared displacement. Finally, based on the Stokes-Einstein equation either the particle size, Diffusion constant D, or temperature T may be calculated.

Latex beads (d= 200 nm and 1000 nm) were coated with S-layers (wtSbpA, SbsB, SatA) and the calculated diffusion coefficient was compared to blank and BSA (as more naturally occurring "blank") coated beads.

The results from the NTA approach with differently coated beads are shown in Fig.36.

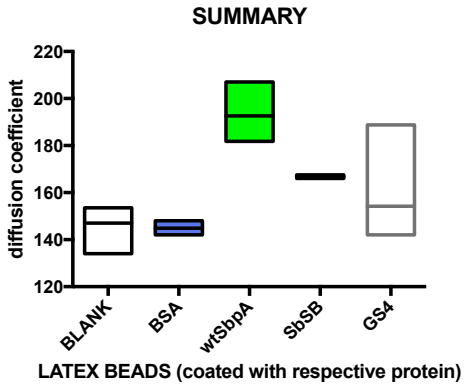

Fig.36 Diagram showing the Diffusion coefficient (in D = 10^{-2} $\mu m^2/s$) versus the differently coated monodisperse particles (d=200 nm).

The wtSbpa coating resulted in higher D values compared to uncoated or BSA coated beads. However, the differences are minimal!

Moreover, the main problem of NTA is the limited depth of view of the light microscope. Most optical methods can achieve high temporal resolution and high localization precision only in two dimensions or over a limited axial (z) range. Nevertheless, particle tracking resembles the natural situation of S-layer coated bacterial cells best and thus seems to be most suitable to study the question of the influence of the flow resistance of S-layers. Thus we have decided to proceed with particle tracking but will make use of a new technique developed at the Institute of Prof. Alberto Diaspro, Istituto Italiano de Technologica (IIT), University of Genoa, Italy which allows real-time volumetric imaging with nanometer precision over extended axial ranges (up to >10 µm in x, y and z). This new technique is explained in detail in ref. [50] .

4.8.1.4. Real-time volumetric imaging of free-diffusing microparticles

Three-dimensional multiple-particle tracking with tunable axial ranges is a novel wide-field detection technique based on an electrically tunable lens. The optical principle of the technique is based on the simultaneous acquisition of two images with an extended depth of field while encoding the z-position of the (light emitting) particles via a lateral shift between images. This approach allows getting nanometric localization precision up to an axial range above 10 µm with a combination of four high numerical aperture lenses which is typical for 3D tracking systems. Synchronization or complex fitting procedures are not required which leads to a suitable architecture for localizing single molecules in three dimensions and real-time. [50]

In these experiments, which had been carried out by Dr. Marti Duocastella, IIT three populations of 1 µm sized fluorescent beads (in water) were examined:

- regular uncoated polystyrene beads
- polystyrene beads coated with crystalline SbpA S-layer protein
- polystyrene beads coated with amorphous SbpA S-layer protein

Fifty trajectories for each population were reconstructed (Fig.37)

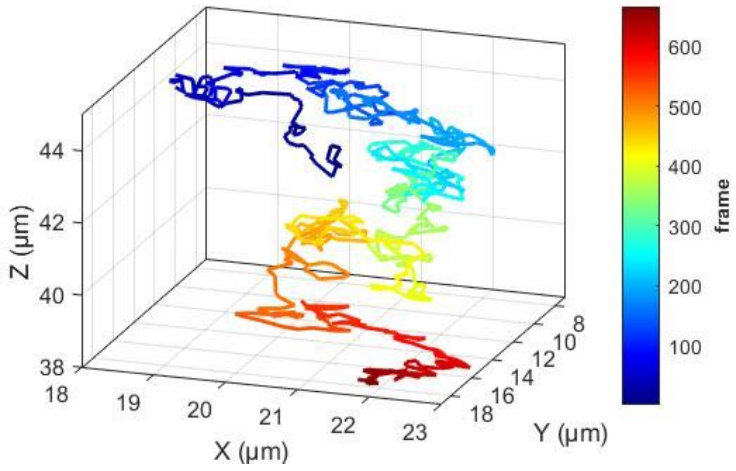

Fig.37 Reconstruction of a particle trajectory after data processing.

For our scientific question, the mean square displacement (MSD) of the particle positions (r) over time (t) had to be determined since this allows us to calculate the respective diffusion coefficients (D).

$$MSD(\tau) = \Sigma\,(r(t+\tau) - r(t))^2$$

where τ is called delay.

A linear fit of the plot MSD *vs.* τ allows to extract the information about the diffusion coefficient D directly:

$$MSD(\tau) = 6D\tau + C$$

In the case of free-diffusing **uncoated beads**, the diffusion coefficient was 0.49 µm^2/s. This is in agreement with the Stokes-Einstein equation where for a 1 µm diameter sized bead in water at 25° C (viscosity of 1.11 mPa•s) the expected diffusion coefficient is 0.49 µm^2/s (Fig.38).

In the case of the **crystalline SbpA S-layer protein-coated beads** the diffusion coefficient, with a value of 0.42 $\mu m^2/s$, was significantly lower than before. Thus it may be concluded that the S-layer applies a dragging force to the particle limiting its movement.

Interestingly, the diffusion coefficient for the beads coated with an **amorphous SbpA S-layer**, with a value of 0.50 $\mu m^2/s$, is comparable to that of the uncoated beads (with a value of 0.49 $\mu m^2/s$).

Thus it was concluded that the lower diffusion coefficient of S-layer coated beads indicates a higher flow resistance for S-layer coated bacterial cells.

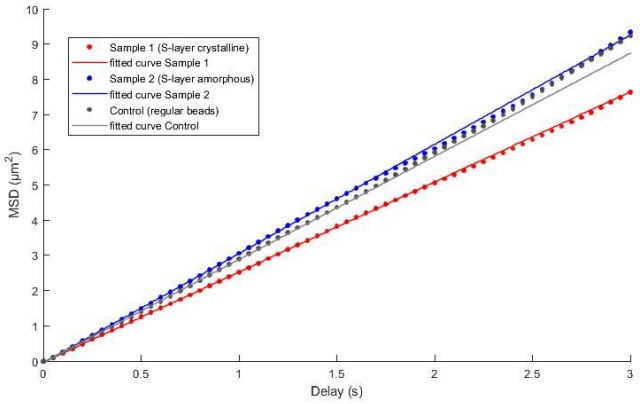

Fig.38 Diagram showing the MSD *vs.* delay (s) for crystalline SbpA S-layer protein coated – (red), amorphous Sbpa S-layer protein coated – (blue), and regular uncoated beads (grey).

4.8.1.5. Zeta Sizer DLS-based optical micro-rheology

Moreover, Zeta Sizer DLS-based optical micro-rheology measurements were performed too. Beads with 200 nm in diameter coated with wtSbpA, SbsB or GS4 were used. Measurements were performed in cuvettes (Fig.39).

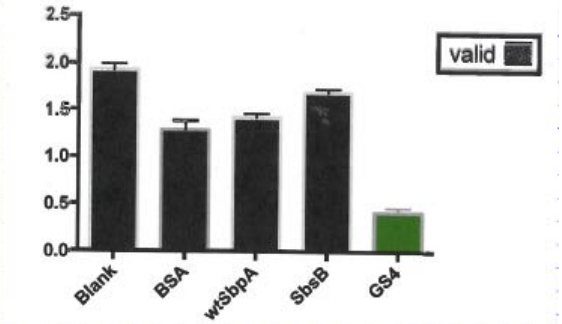

Fig.39 Diagram showing the results from the Zeta Sizer measurements. Diffusion coefficient D in $\mu m^2/s$.

The diffusion coefficients are comparable to the results obtained by NTA. Nevertheless, in this approach the diffusion coefficients for the blank beads are higher than for the S-layer coated ones.

4.8.2. In situ hydrodynamic lateral atomic force microscopy – Optical traps

Originally it was planned that in-situ hydrodynamic lateral force microscopy will be used to study the flow resistance of blank and S-layer coated microbeads because such beads resemble the properties of bacterial cells most closely. Unfortunately, it turned out that our AFM was not able to resolve the minute differences of the frictional forces between uncoated and S-layer coated microbeads which had been glued to the end of the cantilever. However, optical traps (optical tweezers) allow to perform the same measurements but are much more sensitive in determining the minute forces. Thus, we decided to continue with an optical trap for measuring the viscous drag of uncoated and S-layer coated microbeads.

4.8.2.1. Drag experiments with an optical trap (optical tweezers)

Optical traps (also called optical tweezers) use a highly focused laser beam to provide an attractive or repulsive force (typically in the order of pico Newtons) to physically hold and move microscopic dielectric objects such as micro beads.

The idea of the experiment was to measure viscous drag of protein-coated and uncoated beads in a liquid flow (Fig.40). The size of the beads was comparable to the size of bacterial cells.

The flow was established by

- moving the sample with a piezo-table,
- while the bead was trapped ("levitated") by the optical trap at the same position in a sealed sample chamber.

The trap was recalibrated for every bead.

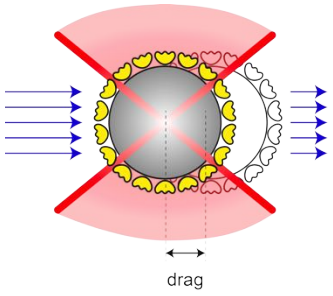

Fig.40 Schematic drawing of the drag experiments.

The piezo table was moved

- 48 µm along the X-axis at a speed of 48 µm/s,
- paused for 0.5 s, and
- subsequently moved back 48 µm at a speed of 48 µm/s.

Drag was calculated as the difference between the mean vales of the force signal for the motion and the pause part (Fig.41).

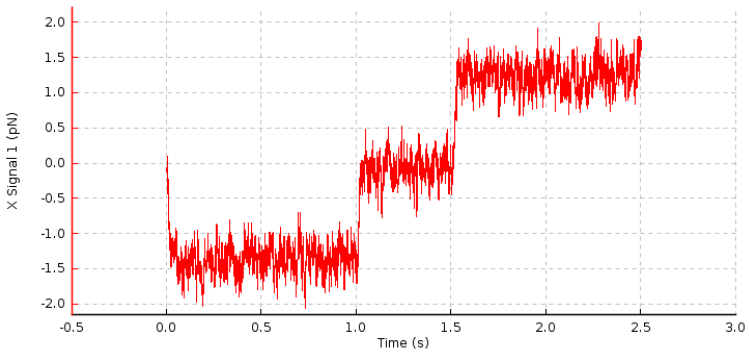

Fig.41 Drag curves (see text for details)

For each new bead measurements were repeated 100 times. In this way, 20,000 data points per sec were sampled. In addition, 50-100 ms at the beginning of each segment were skipped because the signal was affected by the acceleration/deceleration of the piezo-table. Moreover, it was confirmed that each bead was at least 30 µm away from the glass surface in order to be away from the gradient of the flow velocities (Fig.42).

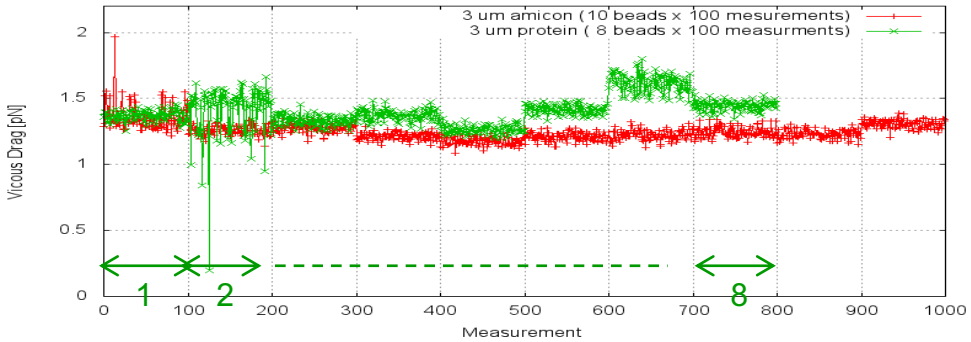

Fig.42 Diagram showing the drag experiments with blank (red; labeled *amicon*) and S-layer coated (green; labeled *protein*) beads. The measurements were repeated eight and ten times, respectively.

As expected, the difference between uncoated and coated beads is very small - if detectable at all! (Fig.43). One could say that S-layer coated beads show a somehow higher friction then uncoated ones. The variation in the measurements may have several factors such as bead size variations or differences in the coating of different beads.

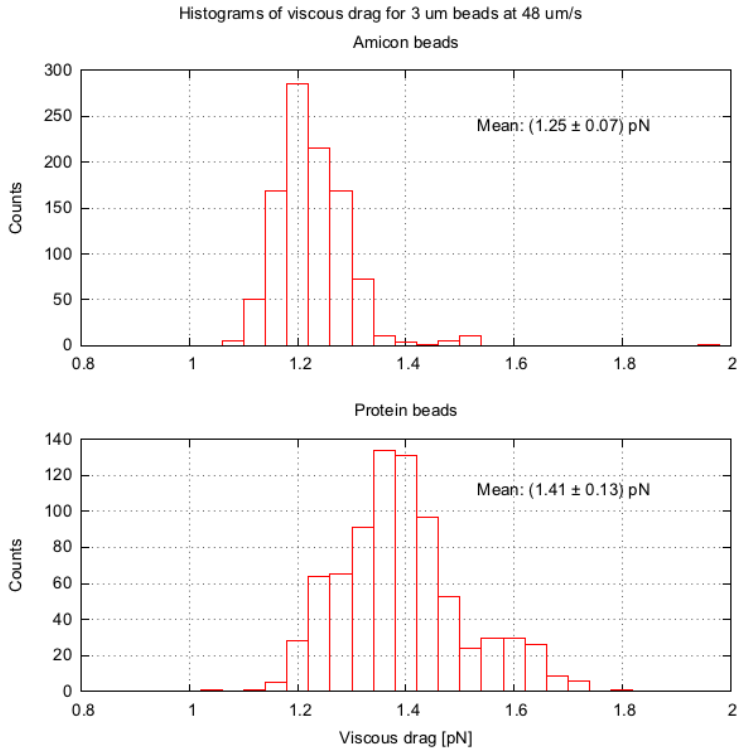

Fig.43 Histograms showing the results of the viscous drag experiments for blank (top; labeled *amicon*) and S-layer coated (bottom; labeled *protein*) beads.

4.8.3. Summary of the flow resistance measurements

Our experiments have shown that the effect of the presence of an S-layer on the flow resistance in water is extremely small. Irrespective of the anti-fouling properties of S-layers it seems that the crystalline lattice increases slightly the flow resistance of bacterial cells in water. Among the different approaches applied to measure the flow resistance or, alternatively the diffusion coefficient, the volumetric imaging technique and the drag experiments with the optical trap seem to be the most precise ones since they resemble the natural situation of a micrometer sized bacterial cell most closely.

4.9. Simulation of flow across an S-layer protein interface

Currently we are focusing on the simulation of flow across S-layers. Although this approach was not contained in the proposal as a separate work package, we are working on a theoretical model which will allow us to get a complete picture of the S-layer - water interface and explain the antifouling and hydrodynamic properties in detail. All simulations were performed by our cooperation partner Dr. Rupert Tscheließnig, University of Natural Resources and Life Sciences, Vienna.

4.9.1. Theory

The dynamics of an incompressible fluid surrounding an object, also like a bacterial cell, is described by the Navier–Stokes equations [51]:

$$\nabla \cdot \boldsymbol{v} = 0$$

$$\rho\left(\frac{\partial \boldsymbol{v}}{\partial t} + (\boldsymbol{v}\cdot\nabla)\boldsymbol{v}\right) = \eta\,\nabla^2 \boldsymbol{v} - \nabla p + \boldsymbol{f}$$

where ρ is the fluid density, η the fluid viscosity, $\mathbf{v}(\mathbf{r},t)$ the position- and time-dependent fluid velocity field, $\mathbf{p}(\mathbf{r}, t)$ the pressure field, and $f(\mathbf{r}, t)$ an applied force. Scaling length, velocity, and time by characteristic values L, $\mathbf{v}_0$, and T_0, respectively, yields

$$\mathrm{Re}_T \frac{\partial \boldsymbol{v}'}{\partial t'} + \mathrm{Re}\,(\boldsymbol{v}'\cdot\nabla)\,\boldsymbol{v}' = \nabla^2 \boldsymbol{v}' - \nabla p' + \boldsymbol{f}'$$

where the prime denotes dimensionless quantities. Re is the classical Reynolds number and Re_T the oscillatory Reynolds number which indicates the importance of the linear unsteady term compared to the viscous term. However, for micro swimmers like bacteria, the Reynolds numbers are very small (for example for a bacterial cell in water, Re = 10^{-3}). In other words, the fluid is extremely viscous for such small objects resulting in a so called Stokes flow, also named creeping flow or creeping motion. In this case the left-hand side of the last equation may be neglected leading to the linearized Stokes equation:

$$\nabla p - \eta\,\nabla^2 \boldsymbol{v} = \boldsymbol{f}$$

A fundamental solution of this equation is called *Stokeslet* which is associated with a singular point force embedded in a Stokes flow.

4.9.2. Software packages

For simulating the flow of water molecules across an S-layer we used molecular dynamic (MD) simulations with lammps (http://lammps.sandia.gov) combined with a Computational Fluid Dynamics (CFD) solver (http://www.nektar.info).

4.9.3. Stokeslets – a fundamental solution of the Stokes equations

The following procedure was used to calculate the (velocity) flow field around various arrangements of Stokeslets (singular point forces):

- First, create Stokeslets, define their coordinates and indicate their initial velocities.
- Then, calculate a Matrix M, describing the force field, and compute the (Penrose) inverted. One obtains forces at the positions of the Stokeslets that keep them at their initial velocity.
- Finally use these forces to compute the flow field.

In Fig.44 the object is represented by Stokeslets (red dots) and moved from left to right or up at 45°, respectively. The gray scale images in (b-d) represent the protein mass distribution of a single unit cell of SbpA as obtained from TEM data under low electron dose conditions and image processing. Protein is light while the pores in the protein lattice are dark. The fluid is at rest in order to eliminate inertial forces.

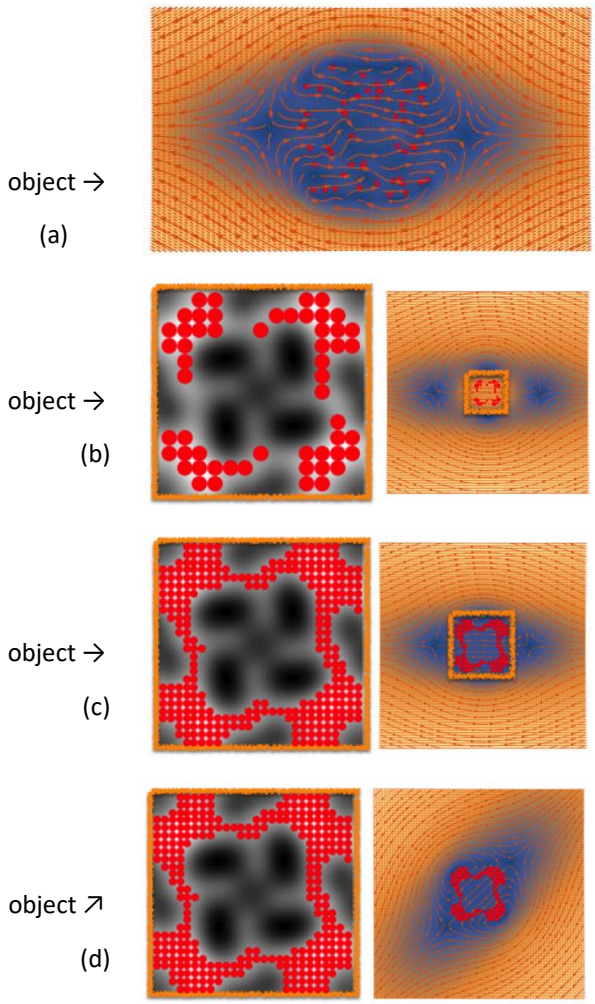

Fig.44 Flow simulations across a random arrangement of Stokeslets (a) and a 2D - SbpA S-layer (b-d). The red dots indicate the Stokeslets. The fluid is at rest and the object moved as indicated. The orange background shows where the flow is high while the blue region indicates reduced or reverse flow.

4.9.4. Summary – Simulations

These preliminary computer simulations are the first results that describe a mean force field to which a potential fluid (water) is exposed to. It resembles flow across the surface of a nanometric S-layer in 2D. These first results indicate a flow reversal across the S-layer pores. It is by far too early to speculate about this effect as a benefit in the metabolism for the bacterial cell.

The S-layer flow model has to be refined in subsequent steps:

- Extension into the third dimension. We expect effects, like micro- or even nano sized turbulences, in the flow field extending into the environment above the S-layer lattice.
- Repetition of the single S-layer unit cell into an extended lattice structure in order to study cooperative effects of the nanometric topography of the S-layer lattice.

- Introduction of functional groups at the S-layer surface, such as negatively charged carboxyl or positively charged amino groups, and at the same time replacing the inert fluid by "real" water molecules. The latter refinement in the simulations might elucidate the role of the "locked-in" water structure as anti-fouling and slippery layer – as assumed in this project as a fundamental beneficial function of the S-layer for the bacterial cell.

Based on the gained experience with SbpA comparative simulations will be carried out with rSbsB, the S-layer protein from *B. stearothermophilus* PV72/p2 which shows oblique (p1) lattice symmetry, and SatA from *Aneurinibacillus thermoaerophilus L420-91* GS4 -97 which is glycosylated and exhibits oblique (p2) lattice symmetry.

4.10. Exploitation and dissemination of the results

The results of this work were published in international SCI-papers (see below) and presented at international conferences and workshops (in most cases as invited speakers). No patent applications at the moment.

5. Summary and Conclusions

Nature has used evolution to build materials that outperform current man-made surfaces and materials. Today we know many examples, such as water repellent surfaces based on the Lotus-leaf effect or spider's hair cells, but little is known about the anti-fouling properties and the flow resistance of bacterial cells - in particular of S-layer coated cells. S-layer proteins are one of the most abundant biopolymers on earth and their synthesis must justify the energy expense by the bacterial cell. Considering the anti-fouling properties and flow resistance of S-layers we presume that besides the more specific functions identified for S-layers of different organisms (e.g. specific interactions with molecules and cell surfaces as observed in pathogens) these features may turn out to be one of the most general ones amongst bacterial and archaeal S-layers. Biomimetic approaches copying these unique S-layer surface properties could be of great technological relevance as already shown in making use of the anti-fouling properties of S-layers in coating the channels of micro fluidic devices. [17-19]

Thus, this research proposal addressed several fundamental questions concerning the anti-fouling properties and the flow resistance of S-layers as benefits for bacterial cells in their natural habitats.

With respect to the contact angle measurements the most important findings were the wetting effect of the crystalline S-layer which switched from hydrophobic for the dry to hydrophilic for the wet S-layer, the importance of the crystallinity of the lattice, and the water-retention capability of S-layers. The latter effect might be of great relevance for bacterial cells in their natural habitats (e.g. soil, mud) since their surface will be kept wet as long as possible when the biofilm is starting to dry out. The hydrophilicity of the wet layered architecture (S-layer and associated water layers) might also explain the higher flow resistance in water as determined in the rheology experiments. Moreover, the oleophobicity of the S-layer may be seen as a further advantage for the bacterial cell in their natural environments since – most likely - the pores in the S-layer will not be blocked. In this context the avoidance of unspecific binding of serum components was demonstrated and might have applications in the development of *in vivo* biosensors or microfluidic devices. [17-19] Moreover, the work on bacterial hydrophobins and the genetic engineering of S-layer fusion proteins belong to the characterization of the antifouling properties of S-layer coated surfaces too. We were surprised that the hydrophobicity of the S-layer-hydrophobin layers was not increased compared to plain S-layer lattices. Although the hydrophobin moiety was fused to the exposed C-terminal end of the S-layer protein it might have been hidden in the folded structure or aggregates might have been formed. However, this questions remains open for the moment.

Moreover, in the framework of this research project we were able to contribute to the model of the non-classical pathway of matrix assembly. [28, 40, 41, 52] The new approach in separating the reassembly process into two distinct steps (adsorption of the protein and reassembly into extended crystalline layers, respectively) offers a much better control and allows to work with much smaller amounts of protein. Both aspects will be highly relevant for applications in biotechnology and biomedicine. In this context, we had been able to establish micro molding in capillaries and micro contact printing as standard procedures for making patterned S-layer lattices. As a result it was possible to demonstrate the adhesive force of the S-layer for water as addressed briefly before. Moreover, although not planned in this research proposal but triggered in the course of the last review meeting, studies on the role of Fe^{2+}-ions for the reassembly process were another important outcome of this project. [48] We could confirm the paleo-geo-chemical hypothesis by which a simple protein membrane generated in the presence of bivalent iron would fulfill barrier and supporting functions in an early (anaerobic) stage of biological evolution [2, 49].

A major part of the work was devoted to the determination of the hydrodynamic surface properties of S-layers. We used several approaches in order to elucidate the question whether the S-layer decreases or increases the flow resistance of bacterial cells in water. Contrary to our original assumption in which the complete S-layer coating would decrease the flow resistance of bacteria and in this way supports flagella-driven cell locomotion, our measurements yielded a slightly increased flow resistance comparted to plain surfaces. However, if the body of the bacterial cell has no friction against the surrounding medium, due to the torque balance it would not move forward at all! It would have to have a keel - as pointed out by Purcell. [53] Otherwise, if friction is too high, the bacterial cell would not move either. We assume that there is a delicate balance between the anti-fouling properties, the flow resistance and the wetting behavior of S-layers which was optimized by nature in the course of evolution. Currently we are focusing on the simulation of water flow across S-layers *in silico* and are confident to answer the question about the flow resistance of S-layer coated bacterial cells soon. In the context of these theoretical studies we will also address the question about the role of those water layers which are closely associated with the nanometric topography and precisely defined repetitive surface chemistry of the S-layer lattice. Although we assume that the switching behavior of the hydrophobicity between the dry and wet S-layer may be explained by first water layers, only theoretical models will allow us to show a complete picture of the S-layer - water interface and explain the antifouling and hydrodynamic surface properties in detail.

The results of this project are primarily relevant for basic research concerning fluid mechanics on molecular scale as determined by the natural S-layer self-assembly system. Nevertheless, we would like to anticipate that the achievements might provide the basis for novel developments in biocompatible non-wetting surfaces as required in micro- or nano total analysis systems (uTAS or nTAS), mass sensitive (bio)chemical sensors, High Throughput Screening (HTS) devices for DNA analysis, or ink jet printing of complex fluids.

6. Appendix – Wetting behavior of smooth and rough surfaces

The fundamental equation that describes a liquid droplet at rest on an ideal, smooth surface is Young's equation, given by:

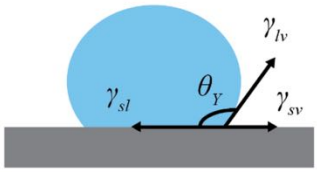

$$\gamma_{sv} = \gamma_{lv} \bullet \cos \theta_Y + \gamma_{sl}$$

where γ_{sv}, γ_{lv}, γ_{sl} are the surface tensions for solid-vapour, liquid-vapour and solid-liquid interfaces, respectively, and θ_Y is the contact angle of the liquid droplet.

For water, when the contact angle is less than 90°, the surface is said to be hydrophilic. Between 90° and 150°, the surface is hydrophobic and above 150°, the surface is defined to be super-hydrophobic. In order to achieve super-hydrophobicity, surface roughness is also required.

There are two main theories that describe the wetting of rough surfaces, namely the **Wenzel** and **Cassie–Baxter models**.

The **Wenzel model** describes homogeneous wetting where the **liquid droplet is in contact with the peaks and valleys of the rough surface**.

For a surface that is intrinsically hydrophilic, $\theta_Y < 90°$, an increasing **roughness factor** renders the surface more hydrophilic, *i.e.*, a decrease in θ_W is observed. Similarly, hydrophobicity can be enhanced with increased roughness for a surface that is intrinsically hydrophobic. However, increases in roughness also increases the solid-liquid interface; hence, the surface in the Wenzel state is **"sticky".** [54]

Wenzel model

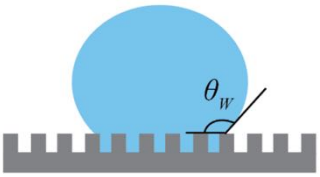

$$\cos \theta_W = R_f \bullet \cos \theta_Y$$

θ_W is the Wenzel contact angle
R_f is the roughness factor

The **Cassie–Baxter** model describes heterogeneous wetting, where the **liquid droplet is suspended by the peaks and does not penetrate into the valleys filled with air**. The Cassie–Baxter equation is derived from Cassie's law, which describes wetting for a two-component surface.

Increasing the area fraction f_1 of air (component 1) will increase the contact angle and reduce the adhesion of the liquid droplet to the surface; thus, the surface is **"slippery".**

Furthermore, even if a material is intrinsically hydrophilic, it can be modified to become hydrophobic by increasing the surface roughness to introduce trapped air pockets.

Cassie–Baxter model

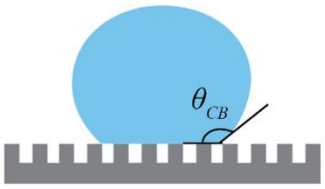

$$\cos \theta_{CB} = f_1 \bullet \cos \theta_1 + f_2 \bullet \cos \theta_2$$

where f_1 and f_2 are the area fractions and θ_1 and θ_2 the contact angles of components 1 and 2, respectively. θ_{CB} is the apparent contact angle of the composite.

However, there may be a transition from the Cassie-Baxter to the Wenzel state. [55]

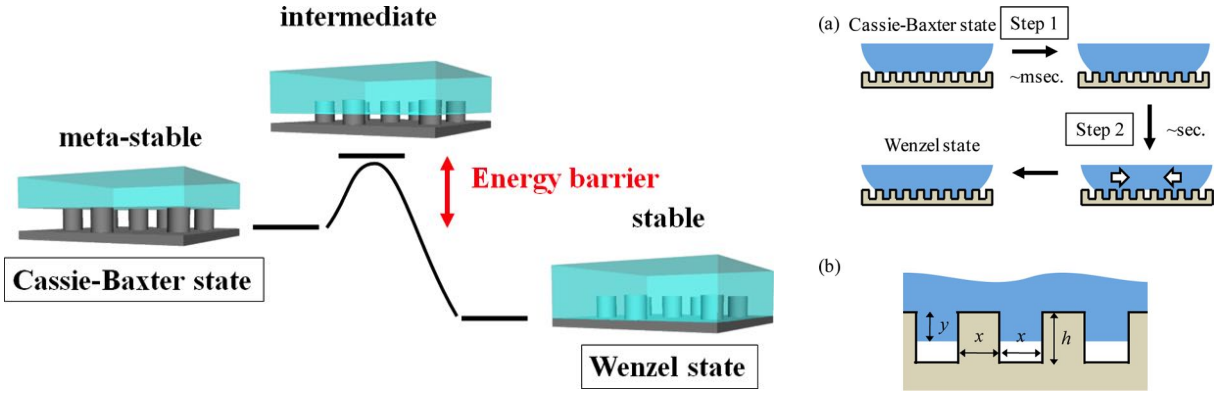

Moreover, introducing a texture with different length scales of roughness can enhance the intrinsic hydrophobicity of a surface. The surface structure of the **rose petal and the lotus leaf** can be used to explain the two different effects. [56]

The red rose takes advantage of this by using a hierarchy of micro- and nanostructures on each petal to provide sufficient roughness for super-hydrophobicity. More specifically, each rose petal has a collection of micro papillae on the surface and each papilla, in turn, has many nanofolds. The water drops maintain their spherical shape due to the super-hydrophobicity of the petal but **do not roll off** because the petal surface has a high adhesive force with water.

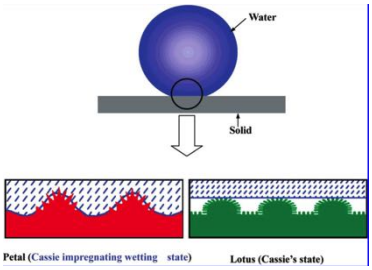

The lotus petal has a randomly rough surface and low contact angle hysteresis, which means that the water droplet is not able to wet the microstructure spaces between the spikes. This allows air to remain inside the texture, causing a heterogeneous surface composed of both air and solid. As a result, the adhesive force between the water and the solid surface is extremely low, allowing the water **to roll** off easily (i.e. "self-cleaning" phenomenon).

7. References

1. Sleytr, U. B., Regular arrays of macromolecules on bacterial cell walls: structure, chemistry, assembly, and function. *Int Rev Cytol* **1978,** 53, 1-62.
2. Sleytr, U. B.; Schuster, B.; Egelseer, E. M.; Pum, D., S-layers: principles and applications. *FEMS Microbiol Rev* **2014,** 38, (5), 823-864.
3. Gruber, K.; Sleytr, U. B., Influence of an S-layer on surface properties of *Bacillus stearothermophilus*. *Arch Microbiol* **1991,** 156, (3), 181-5.
4. Sára, M.; Kuen, B.; Mayer, H. F.; Mandl, F.; Schuster, K. C.; Sleytr, U. B., Dynamics in oxygen-induced changes in S-layer protein synthesis from *Bacillus stearothermophilus* PV72 and the S-layer-deficient variant T5 in continuous culture and studies of the cell wall composition. *J Bacteriol* **1996,** 178, (7), 2108-17.
5. Egelseer, E. M.; Idris, R.; Jarosch, M.; Danhorn, T.; Sleytr, U. B.; Sára, M., ISBst12, a novel type of insertion-sequence element causing loss of S-layer-gene expression in *Bacillus stearothermophilus* ATCC 12980. *Microbiology* **2000,** 146 (Pt 9), 2175-83.
6. Sleytr, U. B.; Glauert, A. M., Analysis of Regular Arrays of Subunits on Bacterial Surfaces - Evidence for a Dynamic Process of Assembly. *J Ultra Mol Struct R* **1975,** 50, (1), 103-116.
7. Sleytr, U. B.; Messner, P., Crystalline surface layers on bacteria. *Annu Rev Microbiol* **1983,** 37, 311-39.
8. Pum, D.; Messner, P.; Sleytr, U. B., Role of the S layer in morphogenesis and cell division of the archaebacterium *Methanocorpusculum sinense*. *J. Bacteriol.* **1991,** 173, (21), 6865-73.
9. Khursigara, C. M.; Koval, S. F.; Moyles, D. M.; Harris, R. J., Inroads through the bacterial cell envelope: seeing is believing. *Canadian journal of microbiology* **2018,** 64, (9), 601-617.
10. Schuster, B.; Sleytr, U. B., Relevance of glycosylation of S-layer proteins for cell surface properties. *Acta Biomater* **2015,** 19, (0), 149-57.
11. Sleytr, U. B.; Sara, M., Ultrafiltration Membranes with Uniform Pores from Crystalline Bacterial-Cell Envelope Layers. *Applied microbiology and biotechnology* **1986,** 25, (2), 83-90.
12. Sára, M.; Sleytr, U. B., Production and characteristics of ultrafiltration membranes with uniform pores from two-dimensional arrays of proteins. *J. Membr. Sci.* **1987,** 33, 27-49.
13. Sára, M.; Sleytr, U. B., Molecular sieving through S-layers of Bacillus stearothermophilus strains. *J. Bacteriol.* **1987,** 169, 4092-4098.
14. Sara, M.; Sleytr, U. B., Charge distribution on the S layer of Bacillus stearothermophilus NRS 1536/3c and importance of charged groups for morphogenesis and function. *J Bacteriol* **1987,** 169, (6), 2804-9.
15. Weigert, S.; Sára, M., Surface modification of an ultrafiltration membrane with crystalline structure and studies on interactions with selected protein molecules. *J Membrane Sci* **1995,** 106, 147-159.

16. Cottin-Bizonne, C.; Barrat, J.-L.; Bocquet, L.; Charlaix, E., Low-friction flows of liquid at nanopatterned interfaces. *Nat Mater* **2003,** 2, (4), 237-240.

17. Rothbauer, M.; Küpcü, S.; Sticker, D.; Sleytr, U. B.; Ertl, P., Exploitation of S-layer Anisotropy: pH-dependent Nanolayer Orientation for Cellular Micropatterning. *ACS Nano* **2013,** 7, (9), 8020-8030.

18. Picher, M. M.; Küpcü, S.; Huang, C. J.; Dostalek, J.; Pum, D.; Sleytr, U. B.; Ertl, P., Nanobiotechnology advanced antifouling surfaces for the continuous electrochemical monitoring of glucose in whole blood using a lab-on-a-chip. *Lab on a chip* **2013,** 13, (9), 1780-9.

19. Rothbauer, M.; Ertl, P.; Theiler, B. A.; Schlager, M.; Sleytr, U. B.; Küpcü, S., Anisotropic Crystalline Protein Nanolayers as Multi-Functional Biointerface for Patterned Co-Cultures of Adherent and Non-Adherent Cells in Microfluidic Devices. *Advanced Materials Interfaces* **2014**, n/a-n/a.

20. Pum, D.; Sleytr, U. B., Large-scale reconstruction of crystalline bacterial surface layer proteins at the air-water interface and on lipids. *Thin Solid Films* **1994,** 244, 882-886.

21. Ilk, N.; Vollenkle, C.; Egelseer, E. M.; Breitwieser, A.; Sleytr, U. B.; Sara, M., Molecular characterization of the S-layer gene, sbpA, of Bacillus sphaericus CCM 2177 and production of a functional S-layer fusion protein with the ability to recrystallize in a defined orientation while presenting the fused allergen. *Appl Environ Microb* **2002,** 68, (7), 3251-3260.

22. Horejs, C.; Gollner, H.; Pum, D.; Sleytr, U. B.; Peterlik, H.; Jungbauer, A.; Tscheliessnig, R., Atomistic structure of monomolecular surface layer self-assemblies: toward functionalized nanostructures. *ACS Nano* **2011,** 5, (3), 2288-97.

23. Sara, M.; Dekitsch, C.; Mayer, H. F.; Egelseer, E. M.; Sleytr, U. B., Influence of the secondary cell wall polymer on the reassembly, recrystallization, and stability properties of the S-layer protein from Bacillus stearothermophilus PV72/p2. *J Bacteriol* **1998,** 180, (16), 4146-53.

24. Schaffer, C.; Muller, N.; Christian, R.; Graninger, M.; Wugeditsch, T.; Scheberl, A.; Messner, P., Complete glycan structure of the S-layer glycoprotein of Aneurinibacillus thermoaerophilus GS4-97. *Glycobiology* **1999,** 9, (4), 407-14.

25. Messner, P.; Pum, D.; Sleytr, U. B., Characterization of the ultrastructure and the self-assembly of the surface layer of Bacillus stearothermophilus strain NRS 2004/3a. *J Ultrastruct Mol Struct Res* **1986,** 97, (1-3), 73-88.

26. Sára, M.; Kuen, B.; Mayer, H. F.; Mandl, F.; Schuster, K. C.; Sleytr, U. B., Dynamics in oxygen-induced changes in the S-layer protein synthesis from Bacillus stearothermophilus PV72 and the S-layer deficient variant T5 in continuous culture and studies of the cell wall composition. *J. Bacteriol.* **1996,** 178, 2108-2117.

27. Novotny, R.; Scheberl, A.; Giry-Laterriere, M.; Messner, P.; Schaffer, C., Gene cloning, functional expression and secretion of the S-layer protein SgsE from Geobacillus stearothermophilus NRS 2004/3a in Lactococcus lactis. *FEMS Microbiol Lett* **2005,** 242, (1), 27-35.

28. Breitwieser, A.; Iturri, J.; Toca-Herrera, J. L.; Sleytr, U. B.; Pum, D., In Vitro Characterization of the Two-Stage Non-Classical Reassembly Pathway of S-Layers. *International Journal of Molecular Sciences* **2017,** 18, (2).

29. Pum, D.; Stangl, G.; Sponer, C.; Fallmann, W.; Sleytr, U. B., Deep UV patterning of monolayers of crystalline S layer protein on silicon surfaces. *Coll. Surf. B* **1997,** 8, 157-162.

30. Wong, T. S.; Kang, S. H.; Tang, S. K. Y.; Smythe, E. J.; Hatton, B. D.; Grinthal, A.; Aizenberg, J., Bioinspired self-repairing slippery surfaces with pressure-stable omniphobicity. *Nature* **2011,** 477, (7365), 443-447.

31. Ulman, A., Formation and Structure of Self-Assembled Monolayers. *Chem Rev* **1996,** 96, (4), 1533-1554.

32. Pavkov-Keller, T.; Howorka, S.; Keller, W., The structure of bacterial S-layer proteins. *Prog Mol Biol Transl Sci* **2011,** 103, 73-130.

33. Ben-Naim, A., *Hydrophobic interactions*. Plenaum press, New York: 1980.

34. Epstein, A. K.; Wong, T. S.; Belisle, R. A.; Boggs, E. M.; Aizenberg, J., Liquid-infused structured surfaces with exceptional anti-biofouling performance. *P Natl Acad Sci USA* **2012,** 109, (33), 13182-13187.

35. Wosten, H. A.; Scholtmeijer, K., Applications of hydrophobins: current state and perspectives. *Applied microbiology and biotechnology* **2015,** 99, (4), 1587-97.

36. Hobley, L.; Ostrowski, A.; Rao, F. V.; Bromley, K. M.; Porter, M.; Prescott, A. R.; MacPhee, C. E.; van Aalten, D. M.; Stanley-Wall, N. R., BslA is a self-assembling bacterial hydrophobin that coats the Bacillus subtilis biofilm. *Proc Natl Acad Sci U S A* **2013,** 110, (33), 13600-5.

37. Brandani, G. B.; Schor, M.; Morris, R.; Stanley-Wall, N.; MacPhee, C. E.; Marenduzzo, D.; Zachariae, U., The Bacterial Hydrophobin BslA is a Switchable Ellipsoidal Janus Nanocolloid. *Langmuir* **2015,** 31, (42), 11558-63.

38. Ilk, N.; Egelseer, E. M.; Sleytr, U. B., S-layer fusion proteins--construction principles and applications. *Curr Opin Biotechnol* **2011,** 22, (6), 824-31.

39. Ferner-Ortner-Bleckmann, J.; Gelbmann, N.; Tesarz, M.; Egelseer, E. M.; Sleytr, U. B., Surface-layer lattices as patterning element for multimeric extremozymes. *Small* **2013,** 9, (22), 3887-94.

40. Chung, S.; Shin, S. H.; Bertozzi, C. R.; De Yoreo, J. J., Self-catalyzed growth of S layers via an amorphous-to-crystalline transition limited by folding kinetics. *Proc Natl Acad Sci U S A* **2010,** 107, (38), 16536-41.

41. Shin, S. H.; Chung, S.; Sanii, B.; Comolli, L. R.; Bertozzi, C. R.; De Yoreo, J. J., Direct observation of kinetic traps associated with structural transformations leading to multiple pathways of S-layer assembly. *Proc Natl Acad Sci U S A* **2012,** 109, (32), 12968-73.

42. De Yoreo, J. J.; Chung, S.; Nielsen, M. H., The Dynamics and Energetics of Matrix Assembly and Mineralization. *Calcif Tissue Int* **2013,** 93, 316-328.

43. Pum, D.; Sleytr, U. B., Reassembly of S-layer proteins. *Nanotechnology* **2014,** 25, (31), 312001.

44. Sleutel, M.; Van Driessche, A. E. S., Role of clusters in nonclassical nucleation and growth of protein crystals. *P Natl Acad Sci USA* **2014,** 111, (5), E546-E553.

45. Jaenicke, R.; Welsch, R.; Sára, M.; Sleytr, U. B., Stability and self-assembly of the S-layer protein of the cell wall of Bacillus stearothermophilus. *Biol. Chem. Hoppe-Seyler* **1985,** 366, 663-670.

46. Krewulak, K. D.; Vogel, H. J., Structural biology of bacterial iron uptake. *Bba-Biomembranes* **2008,** 1778, (9), 1781-1804.

47. Tadolini, B., Iron Autoxidation in Mops and Hepes Buffers. *Free Radical Research Communications* **1987,** 4, (3), 149-160.

48. Iturri, J.; Breitwieser, A.; Pum, D.; Sleytr, U.; Toca-Herrera, J., Electrochemical-QCMD Control over S-Layer (SbpA) Recrystallization with Fe2+ as Specific Ion for Self-Assembly Induction. *Applied Sciences* **2018,** 8, (9).

49. Sleytr, U. B.; Plohberger, R., The dynamic process of assembly of two-dimensional arrays of macromolecules on bacterial cell walls. In *Electron Microsc. at Molecular Dimensions*, Baumeister, W.; Vogell, W., Eds. Springer-Verlag: Berlin, 1980; pp 36-47.

50. Sancataldo, G.; Scipioni, L.; Ravasenga, T.; Lanzano, L.; Diaspro, A.; Barberis, A.; Duocastella, M., Three-dimensional multiple-particle tracking with nanometric precision over tunable axial ranges. *Optica* **2017,** 4, (3), 367-373.

51. Elgeti, J.; Winkler, R. G.; Gompper, G., Physics of microswimmers-single particle motion and collective behavior: a review. *Rep Prog Phys* **2015,** 78, (5).

52. De Yoreo, J., Crystal nucleation: More than one pathway. *Nat Mater* **2013,** 12, (4), 284-285.

53. Purcell, E. M., Life at low Reynolds number. *American Journal of Physics* **1977,** 45, (1), 3-11.

54. Tam, J.; Palumbo, G.; Erb, U., Recent Advances in Superhydrophobic Electrodeposits. *Materials* **2016,** 9, (3).

55. Murakami, D.; Jinnai, H.; Takahara, A., Wetting Transition from the Cassie-Baxter State to the Wenzel State on Textured Polymer Surfaces. *Langmuir* **2014,** 30, (8), 2061-2067.

56. Feng, L.; Zhang, Y. A.; Xi, J. M.; Zhu, Y.; Wang, N.; Xia, F.; Jiang, L., Petal effect: A superhydrophobic state with high adhesive force. *Langmuir* **2008,** 24, (8), 4114-4119.

8. Supported personnel

- Andreas Breitwieser, PhD, Senior Postdoc
- Alberto Moreno-Flores, PhD-student who finished his work in the course of the project.
- Iris Strube, Technician

9. Collaborations

Academia

Dr. Rupert Tscheliessnig, Institute of General Microbiology, University of Natural Resources and Life Sciences Vienna:

Support in the simulation of water flow across an S-layer lattice

Dr. Lucia Terlecki-Zaniewicz, Institute for Biotechnology, Univ. of Natural Resources and Life Sciences, Vienna, Austria:

NTA tracking analysis

Dr. Marti Duocastella, Istituto Italiano de Technologica (IIT), University of Genoa, Italy:

Real time volumetric imaging of free-diffusing nanoparticles

Companies

Dr. Vitaliy Oliynik, JPK Instruments, Berlin, Germany:

Optical tweezers and optical trapping

Dr. Michael Ringhofer and Robert Hammer, Anton Paar GmbH, Graz Austria:

Rheological measurements

10. Publications

- **Iturri, J., Breitwieser, A., Pum, D., Sleytr, U.B., Toca-Herrera, J.L.** 2018. Electrochemical-QCMD control over S-layer (SbpA) recrystallization with Fe2+ as specific ion for self-assembly induction. Appl. Sci. 8:1460
- **Breitwieser, A., Iturri, J. Toca-Herrera, J.L., Sleytr, U.B., Pum, D.** 2017. In vitro characterization of the two-stage non-classical reassembly pathway of S-layers. Int. J. Molec. Sci. 18:400

- **Iturri, J., Vianna, A.C.,Moreno-Cencerrado, A., Pum, D., Sleytr, U.B., Toca-Herrera, J.L.** 2017. Impact of surface wettability on S-layer recrystallization: a real-time characterization by QCM-D. Beilstein J. Nanotechnol. 8:91–98.
- **Damiati, S., Küpcü, S., Peacock, M., Eilenberger, C., Zamzami, M., Qadri, I., Choudhry, H., Sleytr, U.B., Schuster, B.** Acoustic and hybrid 3D-printed electrochemical biosensors for the real-time immunodetection of liver cancer cells (HepG2). Biosensors & Bioelectronics. 94:500-506.
- **Breitwieser, A., Pum, D., Toca-Herrera, J.L. Sleytr, U.B.** 2016. Magnetic beads functionalized with recombinant S-layer protein exhibit high human IgG-binding and anti-fouling properties. Current Topics in Peptide & Protein Research. 17:45-55.
- **Moreno Cencerrado, A. Iturri, J., Pum, D. Sleytr, U.B., Toca-Herrera, J.L.** 2016. Influencing bacterial S-layer protein recrystallization on polymer brushes through surface charge and accessible volume: a combined AFM and QCMD analysis. *Polymer* 102:379-385.
- **Ladenhauf, E.M., Pum, D., Wastl, D.S., Toca-Herrera, J.L., Phan, N.V.H., Lieberzeit, P.A., Sleytr UB.** 2015. S-layer based biomolecular imprinting. *RSC Advances* 5:83558-83564.
- **Melzak, K., Toca-Herrera, J.L.** 2015. Atomic force microscopy and cells: indentation profiles around the AFM tip, cell shape changes, and other examples of experimental factors affecting modelling. Microscop. Res. Techn. 78 (2015) 626

in preparation (tentative list of authors and working titles)

- Breitwieser, A., Sleytr, U. B., Pum, D. Patterning of S-layer lattices
- Duocastelli, M., Breitwieser, A., Sleytr, U. B., Toca-Herrera, J.L., Pum, D. Real-time volumetric imaging of free-diffusing S-layer coated microparticles
- Tscheliessnig, R., Breitwieser, A., Sleytr, U. B., Pum, D. Simulation of flow across an S-layer protein interface

11. Interactions / transitions

--- none ---